UC San Diego
UC San Diego Previously Published Works

Title

Relict landscape resistance to dissection by upstream migrating knickpoints

Permalink

Journal

ISSN

Authors

Brocard, Gilles Y
Willenbring, Jane K
Miller, Thomas E
et al.

Publication Date

DOI

RESEARCH ARTICLE

Key Points:
- Knickpoints in the Luquillo Mountains show consistent, slow retreat at Myr and kyr timescales
- Knickpoint retreat poorly correlates with stream power
- Reduced bed load fluxes from the upstream landscape explain slow knickpoint retreat

Relict landscape resistance to dissection by upstream migrating knickpoints

Gilles Y. Brocard[1], Jane K. Willenbring[1], Thomas E. Miller[2], and Frederik N. Scatena[1]

[1]Department of Earth and Environmental Sciences, University of Pennsylvania, Philadelphia, Pennsylvania, USA, [2]Department of Geology, University of Puerto Rico, Mayagüez, Puerto Rico

Abstract Expanses of subdued topographies are common at high elevation in mountain ranges. They are often interpreted as relict landscapes and are expected to be replaced by steeper topography as erosion proceeds. Preservation of such relict fragments can merely reflect the fact that it takes time to remove any preexisting topography. However, relict fragments could also possess intrinsic characteristics that make them resilient to dissection. We document here the propagation of a wave of dissection across an uplifted relict landscape in Puerto Rico. Using ^{10}Be-^{26}Al burial dating on cave sediments, we show that uplift started 4 Ma and that river knickpoints have since migrated very slowly across the landscape. Modern detrital ^{10}Be erosion rates are consistent with these long-term rates of knickpoint retreat. Analysis of knickpoint distribution, combined with visual observations along the streambeds, indicates that incision by abrasion and plucking is so slow that bedrock weathering becomes a competing process of knickpoint retreat. The studied rivers flow over a massive stock of quartz diorite surrounded by an aureole of metavolcanic rocks. Earlier studies have shown that vegetation over the relict topography efficiently limits erosion, allowing for the formation of a thick saprolite underneath. Such slow erosion reduces streambed load fluxes delivered to the knickpoints, as well as bed load grain size. Both processes limit abrasion. Compounding the effect of slow abrasion, wide joint spacing in the bedrock makes plucking infrequent. Thus, the characteristics of the relict upstream landscape have a direct effect on stream incision farther downstream, reducing the celerity at which the relict, subdued landscape is dissected. We conclude that similar top-down controls on river incision rate may help many relict landscapes to persist amidst highly dissected topographies.

1. Introduction

Perched subdued landscapes are common in mountain ranges. In most cases such landscapes are discontinuous, with fragments of subdued topography surrounded by steeper, more dissected areas. Depending on the setting, they are thought to have formed either directly at high elevation, sometimes at equilibrium with the surrounding landscape, or at low elevation before being uplifted [e.g., *House et al.*, 2001; *Wakabayashi and Sawyer*, 2001; *Anderson,* 2002; *Babault et al.*, 2005; *Garcia-Castellanos*, 2007; *Gunnell et al.*, 2009; *Van der Beek et al.*, 2009; *Brocard et al.*, 2011; *Yang et al.*, 2015]. The latter are viewed as relict landscapes, while surrounding steeper, landscapes are thought to have developed subsequently, as a result of accelerated relative base level fall. Such subdued landscapes are expected to be progressively dismantled and replaced by the surrounding steeper landscapes. However, some perched subdued landscapes have been shown to persist 4 Ma after initiation of dissection [e.g., *Wakabayashi and Sawyer*, 2001; *Van der Beek et al.*, 2009], calling into question the ability for dissection to fully eliminate the relict topography and achieve a new erosional and topographic equilibrium in response to changing climate and tectonics [*Willett and Brandon*, 2002; *Tucker and Whipple*, 2002; *Whipple and Meade*, 2006].

Here we investigate the response of a tropical river system to a step uplift that initiated during the Pliocene. The study site is located on the southern side of the Luquillo Mountains, at the eastern end of Puerto Rico (Figure 1). The island of Puerto Rico lies above a strongly oblique subduction zone. The island has experienced repeated phases of subsidence, standstill, and uplift throughout its geological history. The topography retains extensive shore platforms preserved at high elevation [*Semmes,* 1919; *Lobeck*, 1922; *Meyerhoff*, 1927; *Brocard et al.*, 2015]. The rivers that descend the southern flank of the Luquillo Mountains drain a stock of Eocene-aged quartz diorite. They display pronounced steepened reaches called knickzones or knickpoint faces, delimited upstream by a break in slope called a knickpoint, or knickpoint lip, which can feature waterfalls. The knickpoints found in these rivers do not result from streamwise changes in bedrock resistance. Instead, they cluster in elevation around the elevation of one of these uplifted shore platforms
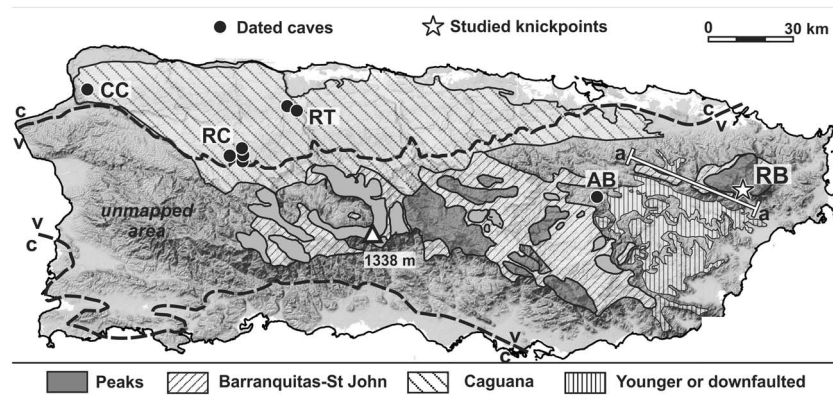
Figure 1. Map of the low-relief surfaces of Puerto Rico, showing the main surfaces identified by *Lobeck* [1922], *Meyerhoff* [1927], ("Caguana" and "Barranquitas"/"StJohn"), and some additional ones ("younger or downfaulted"), showing their extent relative to the Río Blanco river knickpoints (RB) and to the caves dated in this study. Cave groups: AB = Agua Buenas, CC = Cueva Cucaracha, RC = Río Camuy, and RT = Río Tanamá. Dashed lines bound the northern and southern carbonate belts of Puerto Rico (v: volcanic rocks; c: carbonate rocks). Unmapped area: portion of the island where extensive dissection hinders the recognition of low-relief surfaces. a-a': trace of the projected section in Figure 2 (*Brocard et al.* [2015], modified).

and are therefore regarded as the front of a wave of accelerated erosion [*Brocard et al.*, 2015]. They separate an upland relict landscape from downstream bedrock rivers that have incised the shore platform that surrounded the relict landscape. The upland landscape was used in seminal studies to test the validity of the catchment-integrated detrital [10]Be denudation rate method in river-borne quartz [*Brown et al.*, 1995; 1998]. These [10]Be measurements were then combined with measurements of dissolved exports in rivers to propose some of the earliest calculations of long-term weathering fluxes and rates of soil and saprolite development [*White et al.*, 1998; *Riebe et al.*, 2003]. The early isolated measurements were systematized across the relict landscape and expanded to areas located downstream of the knickpoints. They reveal a 30% to 210% increase in soil denudation across the knickpoints [*Brocard et al.*, 2015].

Here we use the differential decay of in situ-produced [10]Be and [26]Al in river-borne quartz buried in caves to date caves that formed shortly after shore platform emergence. These ages are used to approximate when the wave of dissection began and to calculate integrated velocities of knickpoint retreat since initiation. We then use published detrital [10]Be soil denudation rates across the knickpoints to estimate the present-day rates of retreat of these knickpoints and evaluate the consistency between long-term and short-term rates. Both data sets point to slow rates of knickpoint retreat over the past 4 Ma.

We then try to understand why the knickpoints have been retreating so slowly, in the context of a tropical mountain characterized by abundant precipitation and high-intensity storm events. To achieve this, we first look at the distribution of knickpoints expected if knickpoint migration was governed over the long term by stream power-dependent processes such as plucking and abrasion. We conduct a space-for-time substitution, inspecting residuals in arrival time of modeled knickpoints at the places where real knickpoints are observed today instead of looking at spatial differences in the location of modeled and existing knickpoints. We test first a model of knickpoint migration where stream discharge controls migration. We then add the effect of bed load fluxes, bed load grain size, and finally we test a model where incision is controlled by the orientation of joints in the bedrock. We find that the best performing models exhibit a weak dependency on discharge, suggesting a weak control by gravel abrasion and plucking. An inventory of the bed forms carved by the streams into the bedrock along the knickzones is found to be consistent with the conclusions drawn from the knickpoint distribution, with little evidence for gravel abrasion and plucking. Bedrock weathering is extensive in the streambeds along the knickzones and may explain the good performance of the knickpoint distribution model based on the influence of bedrock jointing on knickpoint distribution.

We finally discuss how the bedrock lithology along the knickzones and the soil characteristics upstream of the knickpoints combine here to reduce plucking and bed load abrasion. We generalize these observations by considering which general characteristics of relict topographies may reduce sediment fluxes and slow down the headward migration of knickpoints, helping relict topographies to persist over time.
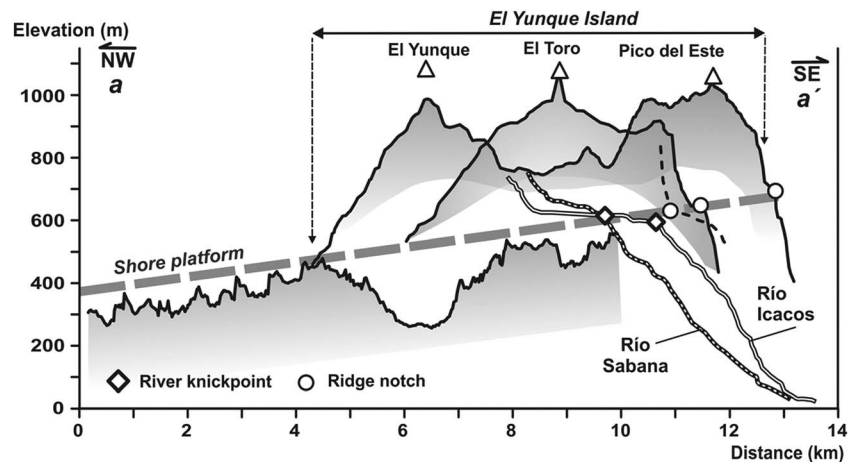
Figure 2. NW-SE projected topographic section across the Luquillo Mountains showing the altitudinal correspondence between the tilted Barraquitas-Caguana shore platform, the protruding "El Yunque Island," and the knickpoint lips in two tributaries of the Río Blanco (*Brocard et al.* [2015], modified). See Figure 1 for location.

2. Knickpoint Generation in the Luquillo Mountains

Puerto Rico and the Virgin Islands comprise the emergent portion of an almost rigid tectonic block located at the NW corner of the Caribbean plate [*Mann et al.*, 1995; *ten Brink et al.*, 2009]. The block is made of island-arc volcanic rocks erupted between the Late Jurassic and the Paleogene. Volcanic activity ended with the collision of the arc with the Bahamas Bank in Early Eocene time [e.g., *Rojas-Agramonte et al.*, 2008; *Stanek et al.*, 2009]. The collisional orogen soon eroded away and became a slowly subsiding platform experiencing dominantly terrigenous sedimentation during the Oligocene. Reefal sedimentation became dominant during Miocene time [*Monroe,* 1980a, *van Gestel et al.*, 1999]. Reefal sedimentation ended during the early Pliocene with deposition of pure carbonates [*Moussa et al.*, 1987]. However, still in the early Pliocene, the Virgin Islands-Puerto Rico tectonic block experienced a rapid northward tilting of 4° [*Moussa et al.*, 1987; *van Gestel et al.*, 1998; *ten Brink,* 2005]; the northern edge of the platform sank 4.5 km into the Puerto Rico Trench while its southern ledge emerged. The carbonate cover on the emergent side of the block started eroding, exposing the underlying volcanic basement. Today, the exposed volcanic basement culminates at 1300 m above sea level. Vast expanses of flat, subhorizontal erosional surfaces in various stages of dissection are found between 100 m and 900 m in elevation (Figure 1 and the supporting information). They can be identified in the topography as areas of subdued topography (see supporting information Figure S1). These prominent surfaces were first surveyed by *Semmes* [1919] and *Lobeck* [1922]. *Semmes* [1919] interpreted them as remnants of a large peneplain, exhumed from beneath the Oligocene-Miocene reef cover. The progressive decline of the terrestrial sources in the Miocene reef platform [*Briggs,* 1966; *Monroe,* 1980b] was attributed to a decrease in erosion rate during the formation of these surfaces [*Monroe,* 1980b]. *Meyerhoff* [1927] found that the tilted Oligo-Miocene platform was truncated by one erosional surface ("Caguana surface," Figure 1) and concluded that the surfaces formed after the initial tilting of carbonates, later ascribed to the Pliocene. Similar flat-lying erosional platforms are found at a depth of 100 m around Puerto Rico and the Virgin Islands, where they also bevel both the basement and the overlying carbonates [*van Gestel et al.*, 1998]. The Puerto Rican uplifted peneplains are therefore more likely marine shore platforms, an interpretation supported by the widespread occurrence of allochthonous sediments dispersed over the uplifted surfaces, and also compatible with the very short time during which these surfaces were allowed to form [*Brocard et al.*, 2015].

Remnants of one such platform fringe the Luquillo Mountains on several sides [*Lobeck,* 1922] (supporting information S2-1). They enclose an ancient "El Yunque" Island, 10 km in diameter and 500 m high (Figure 2), similar in size and height to the islands found in the Virgin Islands archipelago [*Brocard et al.*, 2015]. The platform rises to the ESE with an inclination of 0.7° and projects across the Luquillo Mountains within an elevation range of 500 to 650 m. Flat topographic shoulders, notches on ridges, and knickpoint lips are found around the Luquillo Mountains at the elevation of the projected platform (Figure 2). The most dramatic knickpoints (Figure 3) are observed along the tributaries of Río Blanco, a river that drains a stock of massive quartz diorite.
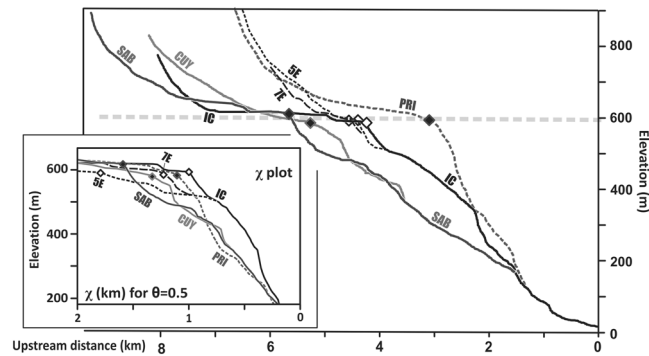
Figure 3. Longitudinal (long) river profiles of the main branches of Río Blanco, with locations of knickpoint lips (diamonds). Tributary names: CUY = Cubuy, IC = Icacos, PRI = Prieto, SAB = Sabana, and 5E and 7E = east tributaries of Río Icacos. Inset: χ plot of the same river profiles [*Perron and Royden*, 2012], with χ calculated for a reference drainage area A_o of 1 km² and an intrinsic concavity of 0.5. The χ scale is a drainage area-weighted upstream distance representation of river profiles in which knickpoints retreating at a celerity solely controlled by drainage area plot at the same χ distance. This representation highlights how K_{IC} lags behind other knickpoints (see section 5).

Above the knickpoints, rivers have concave-up alluvial reaches with low gradients and limited stream power [*Pike et al.*, 2010]. Along the knickpoint faces, streams flow directly over bedrock. The knickpoint lips are located entirely within the homogeneous interior of the quartz diorite stock and cluster around the 600 m altitude of the uplifted shore platform. Their presence is therefore interpreted as the front of a headward migrating wave of incision propagating along the branches of Río Blanco, as a consequence of the uplift that brought the 600 m platform from sea level up to its present-day elevation [*Brocard et al.*, 2015]. Coastal plains around the Luquillo Mountains are devoid of old (>20 kyr) terrace tracts (A. Johnson, ¹⁴C ages, Río Fajardo alluvial plain, unpublished data, 2005), and the surrounding

shelf is devoid of raised reefs, suggesting a lack of late Quaternary uplift. Fault scarps around the Luquillo Mountains are also highly degraded, suggesting that differential tectonic activity has ceased, at least during the past few hundreds of thousands of years. The streams of the Luquillo Mountains have been classified as "flood dominated" channels. Floods are intense and peak discharges can be 1000 times greater than base flow. Peak flow hydrographs are short-lived and typically have a duration of less than 1 h. Stormflow runoff is quickly flushed through the system such that the streams return to base flow within 24 h of large events [*Murphy and Stallard*, 2012]. Discharges close to the annual peak are experienced several times in a year [*Pike et al.*, 2010; *Phillips et al.*, 2013].

3. Methods

3.1. In Situ-Produced Cosmogenic ¹⁰Be and ²⁶Al in Quartz

We measured in situ-produced cosmogenic ¹⁰Be and ²⁶Al in river-borne quartz deposited in caves along the karstified northern carbonate belt of Puerto Rico (see section 4.1). Terrestrial cosmogenic ¹⁰Be and ²⁶Al are produced in quartz lattices during the exhumation of quartz crystals through the uppermost few meters beneath the Earth's surface. Cosmogenic production during subsequent downslope transport, fluvial transport, and transitory storage in floodplains is generally regarded as minimal compared to the initial exhumation [*Schaller et al.*, 2001]. Once buried in a cave, ²⁶Al/¹⁰Be decreases due to faster decay of ²⁶Al compared to ¹⁰Be (half-lives of 0.71 and 1.4 Myr, respectively). The concentration of these isotopes in buried quartz grains can thus be used to retrieve the minimal burial age of the sediments [*Lal*, 1991; *Granger and Muzikar*, 2001].

We extracted sand from gravelly and sandy layers deposited within or near ancient subterranean river channels. The ¹⁰Be-²⁶Al-derived burial age represents a minimum age for the formation of the surrounding conduit and probably represents the moment when the river occupying the conduit was rerouted into a deeper level. We avoided silty sand sequences deposited above the coarse basal deposits because they may have been deposited during floods tens to hundreds of thousands of years after the initial abandonment of the conduit, or during the temporary choking of deeper conduits.

Samples were prepared at the University of Pennsylvania Cosmogenic Isotope Laboratory. Sand and gravels were cemented by carbonates, iron, and manganese oxides that were eliminated using hydrochloric acid. The loosened sediment was then sieved into phi-scale size fractions. Quartz isolation, purification, and dissolution; ion exchange extraction; and precipitation of beryllium were performed following an adaptation of the technique of *Kohl and Nishiizumi* [1992]. Inductively coupled plasma optical emission spectroscopy measurements indicate that total Al concentration in quartz after etching was higher in the standard fraction

Table 1. [10]Be and [26]Al Concentrations and Burial Age of Quartz in Caves[a]

Cave	Grain Size (ϕ)	Easting (deg)[b]	Northing (deg)[b]	Altitude (m)[b]	[[10]Be] 10^4 at g^{-1}	[[26]Al] 10^4 at g^{-1}	[26]Al/[10]Be	Burial Age(Myr)
CUC	3–2	−67.135	18.418	130	24.36 ± 0.52	110 ± 12.9	4.5 ± 0.5	0.8 ± 0.1
HUM (c)	−3–4	−66.830	18.316	290	5.89 ± 0.22	5.57 ± 2.68	0.9 ± 0.5	4.0 ± 2.0
ENS (c)	0–1	−66.824	18.323	310	6.46 ± 0.45	7.76 ± 0.54	1.20 ± 0.12	3.6 ± 0.4
	4–2				7.44 ± 0.40	6.96 ± 0.47	0.94 ± 0.08	4.0 ± 0.4
LAR (c)	1–0	−66.814	18.320	330	3.40 ± 0.21	2.50 ± 0.32	0.74 ± 0.10	4.5 ± 0.6
OSC (c)	1–0	−66.822	18.322	340	5.45 ± 0.29	4.11 ± 0.36	0.75 ± 0.08	4.5 ± 0.5
JAG (t)	−3–4	−66.691	18.396	30	3.82 ± 0.19	2.52 ± 5.6	0.7 ± 0.2	4.7 ± 1.0
	4–2				4.43 ± 0.38	3.56 ± 0.37	0.80 ± 0.11	4.4 ± 0.6
SOR (t)	4–2	−66.723	18.407	100	3.91 ± 0.30	2.86 ± 0.28	0.73 ± 0.09	4.6 ± 0.6
ABU	−3–4	−66.108	18.231	280	5.20 ± 0.26	4.81 ± 0.88	0.93 ± 0.18	4.1 ± 0.8

[a]Cave names: CUC = Cucaracha, HUM = Humo, ENS = Ensueño, LAR = Larga, OSC = Oscura, JAG = Jaguar, SOR = Sorbeto, and ABU = Agua Buenas. Cave groups: (c) = Camuy and (t) = Tanamá.
[b]Location of cave entrances (purposely imprecise for the sake of cave preservation). Analyzed sediment grain size fraction given in phi scale with particle diameter $D = D_o 2^{-\phi}$ with $D_o = 1$ mm.

(0.25–0.5 mm) than in the 0.5–1.0 mm and 1–2 mm fractions, which were used to gain dating precision. Selected fractions had Al concentration ranging from 25 to 90 ppm that did not necessitate [27]Al carrier addition. About 220 μg of [9]Be carrier (Scharlau BE03450100 carrier batch 2Q2P—14 October 2010) with a measured [10]Be/[9]Be ratio of $1.5 \cdot 10^{-15}$ was added to each sample during quartz dissolution. Ti and Fe were precipitated at pH 13 and removed prior to the ion exchange chromatography separation of Be and Al. Be and Al hydroxides were precipitated at pH 8–9, oxidized to BeO and Al_2O_3 over an open butane-propane flame and mixed with Nb and Ag, respectively. The [10]Be/[9]Be and [26]Al/[27]Al ratios were measured by accelerator mass spectrometry at PRIME Laboratory, Purdue University. Results were normalized to standard 07KNSTD for [10]Be and 319500KNSTD for [26]Al [*Nishiizumi et al.*, 2007; *Balco et al.*, 2008] with an assumed [10]Be/[9]Be ratio of $2.79 \cdot 10^{-11}$ [*Balco*, 2009]. [10]Be/[9]Be and [26]Al/[27]Al ratios of the procedural blanks were 2.8 ± 0.8–$3.4 \pm 0.7 \cdot 10^{-15}$ and $2 \pm 6 \cdot 10^{-15}$, respectively. Reported 1 sigma uncertainties (Table 1) encompass uncertainties on Purdue accelerator mass spectrometry measurement, uncertainties on the primary standard, an estimated 2% uncertainty on the Be concentration of the carrier solution, and uncertainties on the procedural blanks. The production ratio of [26]Al/[10]Be and the decay constants are those used in the CHRONUS online calculator [*Balco et al.*, 2008] version 2.2.1 [*Balco*, 2009].

3.2. Digital Extraction of Knickpoints

The river profiles of the six main branches of Río Icacos were extracted from a 1 m lidar digital elevation model (DEM) (doi: 10.5069/G9BZ63ZR) resampled at 5 m to eliminate DEM artifacts due to poor differentiation of canopy and corestones. Cloudiness prevented lidar acquisition over 5% of the catchment of Río Blanco. Void areas were patched using a 10 m DEM generated by interpolation of 10 m elevation contour lines [*Pike et al.*, 2010]. Drainage lines were defined using Arc Hydro Tools 2.0 operated under ArcGIS 10.0 [*Maidment*, 2002]. Elevation and drainage area were extracted along the river paths using extraction module ETsurface for ArcGIS (http://www.ian-ko.com) and transferred to Excel for the modeling of knickpoint propagation. Knickpoint lips are defined as major, irreversible downstream increases in river gradient. In the field, they correspond to the transition from alluvial to bedrock reaches, and their locations are known to within ± 10 m. Corestone accumulations are observed upstream of the knickpoint lips, along five of the studied knickpoints; they impede water flow and generate short (<150 m long) oversteepened reaches along three of the studied streams. These oversteepened reaches are located within 270–650 m of the main knickpoint lips, from which they are separated by alluvial reaches. We therefore hypothesize that rather than drawdown reaches, they correspond to a zone where floodplain groundwater is forced up into the streams due to shallowing bedrock, increasing pore pressure, landsliding, and sapping at the toe of the valley slopes, thereby enhancing delivery of corestones to the streambed.

3.3. Bed Load Grain Size Analysis

For the purpose of investigating the effect of bed load grain size on knickpoint retreat rates, we measured streambed grain size immediately upstream of the knickpoints. Streambed grain size distributions are commonly bimodal, peaking in the sand and in the gravel classes separated in a saddle centered around 1–4 mm
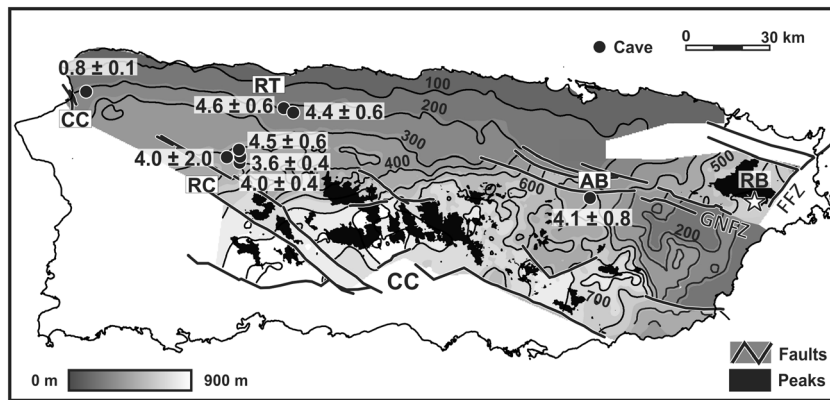
Figure 4. Finite uplift and age of the shore platforms. Location and age of dated caves (groups: AB = Agua Buenas, CC = Cueva Cucaracha, RC = Río Camuy, and RT = Río Tanama). Star RB: Río Blanco drainage. A surface envelope contoured every 100 m was fitted over the remnants of shore platforms (Figure 1). Mountains protruding above the platforms are displayed in black (CC: Central Cordillera). A 210 m diameter filter extracting maximum elevation was passed over the platform remnants to remove the effects of karstification and regolith dissection. The surface envelope was built by fitting a "spline with barriers" interpolation to the extracted elevations. During the interpolation, major tectonic faults such as the Great Northern Fault Zone (GNFZ) or the Fajardo Fault Zone (FFZ) can be used as "barriers" that offset the surface, wherever their introduction statistically improves the fit (Brocard et al. [2015], modified).

[*Kellerhals and Bray*, 1971]. Because bedrock erosion is predominantly achieved by the coarse fraction of the bed load [e.g., *Whipple et al.*, 2000], we sampled gravel bars displaying recent evidence of mobility and excluded the sand fraction. *Wolman* [1954] pebble counts of 100 grains were conducted on bar surfaces and were complemented by photo sieving. Five to 12 images were acquired on each bar, 50 cm to 2 m above the bar surfaces, depending on median clast size. Images were processed using the Cobblecam software [http://walrus.wr.usgs.gov/staff/jwarrick], which calculates D_{50} values by autocorrelation of digital images [*Warrick et al.*, 2009]. Comparison of manual measurements and digital measurements was used to correct autocorrelation measurements for a 7% bias in the estimate of the median grain size.

4. Knickpoint Initiation and Retreat

4.1. Age of Initiation of Uplift and Knickpoint Nucleation

The ^{10}Be-^{26}Al burial dating of caves in northern Puerto Rico allows us to constrain the timing of knickpoint nucleation along the Río Blanco drainage. Emergence of the shore platforms that had formed during the Pliocene exposed the underlying Mio-Pliocene carbonates, affecting the large aquifer that they host [*Giusti*, 1978; *Renken et al.*, 2002]. Emergence forced the rivers that drain the Central Cordillera of Puerto Rico to expand downstream across the newly emerged platforms. The largest rivers incised throughgoing canyons, drawing down the water table and allowing for karstification to initiate in the nonsaturated zone above the water table. The smaller rivers sank into the carbonates, leaving dry valleys and doline lineaments over their karstified surface, and opened extensive karst conduits [*Monroe*, 1976; *Troester*, 1994; *Miller*, 2004]. As incision continued, early conduits were abandoned and replaced by deeper river courses, some of which are still active today. Epikarstification at the surface of the platform then led to the development of a very serrated polygonal cockpit karst [*Monroe*, 1976], characterized by tall cones (mogotes) that reach 100 to 140 m in height above the Cucaracha and Camuy cave systems. Epikarstification led to the exposure of the cave segments studied here (Camuy, Cucaracha, and Agua Buenas groups), while others were exposed due to the cutting of slot canyons (Tanama group). Ten out of the 13 of the targeted caves contained sand and gravel that yielded quartz in a size fraction suitable for the analysis (0.25–2 mm). These caves belong to four systems which are, from west to east, the Cueva Cucaracha, Río Camuy, Río Tanama, and Agua Buenas groups (Figures 1 and 4). The Cucaracha and Tanama groups have developed into the lower Miocene Aguada and Montebello limestone members; the Camuy group is hosted by the upper Oligocene-lower Miocene Lares limestone member [*Monroe*, 1980a; *Troester*, 1994; *Miller*, 2004], while the Agua Buenas group has developed into an isolated patch of Cretaceous reefal limestones embedded into country volcanoclastic rocks. The quartz extracted from these caves tracks from dioritic and quartz dioritic stocks located in the Central

Cordillera of Puerto Rico, where they intrude Jurassic and Cretaceous volcanoclastics poor in quartz in the analyzed grain size fraction [*Seiders*, 1971; *Briggs and Aguilar-Cortés*, 1980; *Buss et al.*, 2013]. In Cueva Cucaracha, however, one potential source of quartz is the Oligo-Miocene San Sebastian shale which happens to contain sandy and conglomeratic members in that specific area [*Monroe*, 1980a].

^{10}Be-^{26}Al burial ages (Table 1) indicate that all caves except Cueva Cucaracha formed in the early Pliocene. Pliocene cave ages are remarkably similar. The strong clustering of the ages advocates for an overestimation of the analytical uncertainties and for synchronous emergence of the shore platforms during the early Pliocene. No spatial trend in emergence time is evident nor is the temporal resolution and limited number of dated sites sufficient to allow the identification of an age difference between the "Barranquitas" ($n = 8$) and "Caguana" ($n = 1$) surfaces of *Meyerhoff* [1927]. Lumping the ages together provides a mean age of 4.2 $\pm$ 0.3 Myr for the initiation of platform uplift.

These burial ages are compatible with the geological constraints on the topographic evolution of Puerto Rico. The latest carbonate to have been deposited onto the Mio-Pliocene platform is the Quebradillas member [*Seiglie and Moussa*, 1975; *Moussa et al.*, 1987]. The Quebradillas member is encountered offshore all across the platform, indicating that platform tilting occurred after its deposition [*Moussa et al.*, 1987; *ten Brink*, 2005]. Sedimentation of the Quebradillas limestone is also marked by a 200 m increase in accommodation space that contrasts with earlier sedimentation and could be related to the tilting [*Seiglie and Moussa*, 1975]. It contains fossils of *Globorotalia tumida tumida* (now *Globorotalia merotimuda*) which appeared 5.6 Myr ago and *Globorotalia margaritae* which appeared 6.0–6.4 Myr ago [*Hayward et al.*, 2015]. This suggests that platform tilting predates cave formation by 1.2 $\pm$ 0.3 Myr. The shore platforms that beveled the carbonates and the volcaniclastic basement may have started forming either during [*Monroe*, 1980a] or immediately after the deposition of the latest carbonates [*Meyerhoff*, 1927]. The shore platform would have to have developed landwards at an average rate of 17.0 $\pm$ 1.2 mm/yr to bevel the carbonate platform to its currently exposed width, assuming that planation spanned the time between the early Pliocene tilting event and the burial of quartz-bearing sediment into the caves. Such a rate is consistent with modern measurements of 18–35 mm/yr sea cliff retreat rates in similarly poorly consolidated carbonates [e.g., *Dornbusch et al.*, 2008; *Letortu et al.*, 2014] and 14.3 mm/yr in flysh [*De Lange and Moon*, 2005]. Beveling of the volcanoclastic basement could require more time, as reported rates of long-term cliff retreat in volcanic rocks are generally lower (0.6–1.7 mm/yr [*Smoot*, 1995; *Mitchell et al.*, 2003]). However, high rates of 10–30 mm/yr have also been reported in volcanic rocks [*Mackey et al.*, 2014]. One age outlier is Cueva Cucaracha. Samples were collected closer to the modern stream level and therefore may simply date a younger conduit. It is noticeable, however, that no quartz-bearing formations are currently exposed in the restricted headwaters of its subterranean system. The burial age therefore provides a minimum age for the capture of the quartz-feeding headwaters of that cave by west flowing rivers [*Miller*, 2007] south of the cuesta that marks the southern border of the tilted reefal platform (Figure 1). Land emergence and drainage rearrangement in that area may be more recent and result from the offshore opening of the Mona Rift, west of Puerto Rico, responsible for the activation of faults on land near Cueva Cucaracha [*Hippolyte et al.*, 2005; *Miller*, 2007].

4.2. Consistency Between Longer-Term and Shorter-Term Knickpoint Retreat Rates

We take the minimum age of emergence of the shore platforms provided by cave dating as the age of initiation of the knickpoints found along Río Blanco. The knickpoints may have initiated at the ledge of the shore platform, or at tectonic dislocations within the platform. The Luquillo Mountains are bounded by fault zones that separate the mountains from the surrounding coastal foothills and from similar shore platforms still below sea level located between the Luquillo Mountains and the Virgin Islands [*Brocard et al.*, 2015; *van Gestel et al.*, 1998]. The closest place to the mountain front that is likely to have experienced tectonic dislocation is located at the intersection between the Great Northern Fault Zone and the Fajardo Fault zone, which bound the mountains to the southwest and southeast respectively (Figure 4 and supporting information Figure S2-1). Concordant remnants of shore platform within the watershed indicate that tectonic disruptions of stream profiles did not occur farther upstream. The location of these faults is therefore used as the site where these knickpoints were generated. It also corresponds to the southernmost extent of the Río Blanco stock, meaning that knickpoint propagation has taken place mostly within the massive dioritic stock, rather than within the more heterogeneous surrounding volcanoclastics. Using such assumptions, we find that the Río Blanco knickpoints have retreated only 5–7 km over the past 4.2 $\pm$ 0.3 Myr at a time-integrated celerity of 1.1 to 1.5 mm/yr.
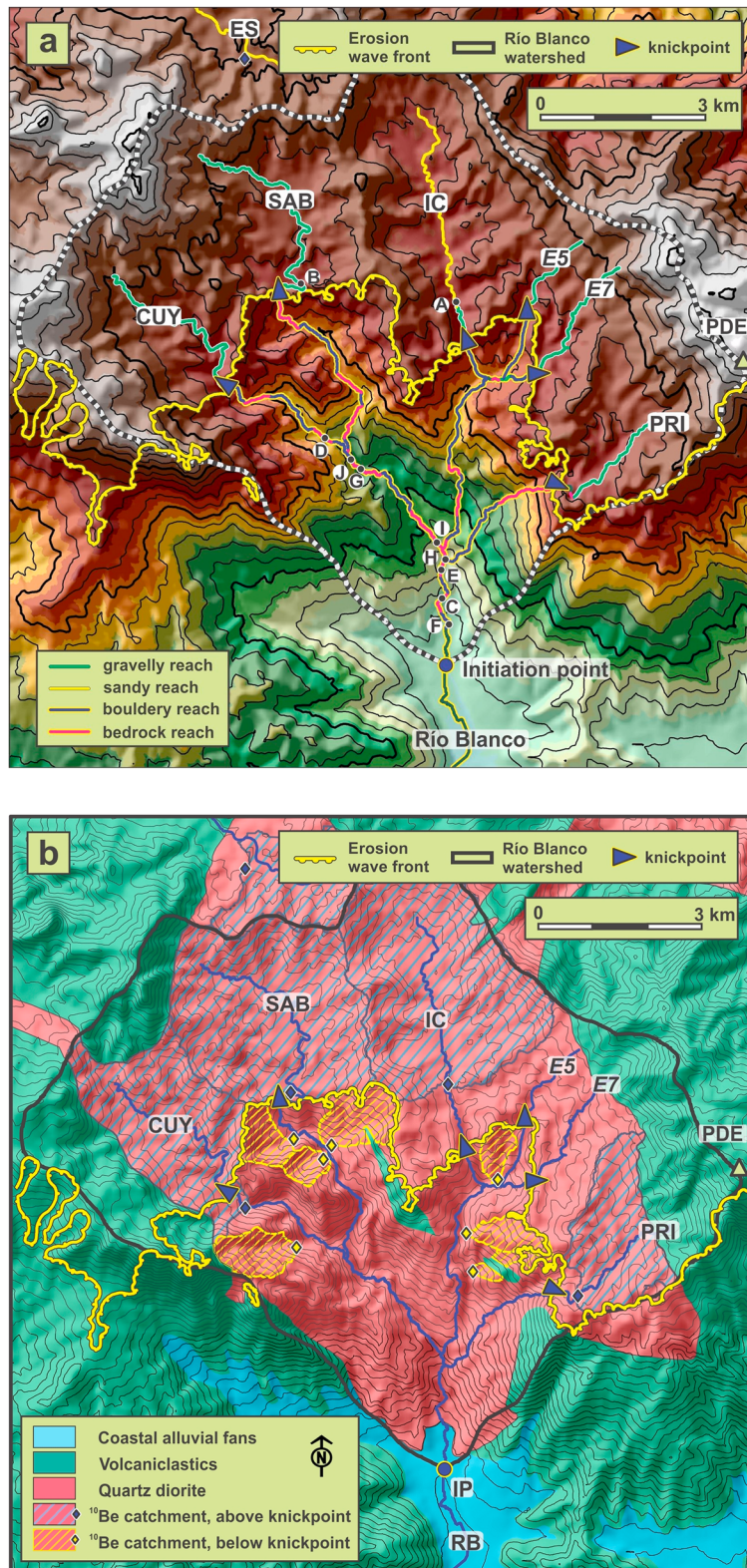
Figure 5. (a) Topography and (b) geology of the Río Blanco catchment, showing features used for modeling of knickpoint retreat such as the Cubuy (CUY), Sabana (SAB), Icacos (IC), Prieto (PRI) branches of the Río Blanco netwrok, and Icacos tributaries E5 and E7. Figure 5a shows the location (A–J) of the field photographs of Figure 9. Figure 5b shows the catchments used to measure erosion upstream and downstream of the knickpoints [*Brocard et al.*, 2015]. Topographic contour spacing is 50 m (Figure 5a), and 25 m (Figure 5b), from 25 m to 1050 m at Pico del Este (PDE).

Table 2. [10]Be-Derived Catchment-Wide Denudation Rates and Increase in Erosion Rate Across the Knickpoints[a]

	Erosion Upstream, All Data Set (m/Myr)		Erosion Downstream, All Data Set (m/Myr)		Erosion Increase, All Data Set (x Upstream)		Erosion Increase Across K_{IC} (x Upstream)		Erosion Increase Across K_{SAB} (x Upstream)	
	c	f	c	f	c	f	c	f	c	f
No corrections	116 ± 7	31 ± 1	247 ± 12	53 ± 2	2.1 ± 0.2	1.7 ± 0.1	1.7 ± 0.3	1.4 ± 0.2	2.6 ± 0.6	2.5 ± 0.6
1 + topography + vegetation shielding	104 ± 6	29 ± 1	225 ± 11	49 ± 2	2.2 ± 0.2	1.7 ± 0.1	1.7 ± 0.3	1.4 ± 0.2	2.7 ± 0.6	2.5 ± 0.6
2 + quartz enrichment + ground density	81 ± 5	48 ± 2	175 ± 8	64 ± 2	2.2 ± 0.2	1.3 ± 0.1	1.7 ± 0.3	1.1 ± 0.1	2.7 ± 0.6	2.0 ± 0.5
3 + time dependence of [10]Be production	84 ± 6	53 ± 2	176 ± 8	70 ± 3	2.1 ± 0.3	1.3 ± 0.1	1.7 ± 0.4	1.1 ± 0.1	2.6 ± 0.7	1.9 ± 0.5

[a]Reported values for "all data set" entries are averages of detrital [10]Be denudation rates from Brocard et al. [2015] for five catchments located upstream of the knickpoints and seven catchments located downstream of the knickpoints. The increase in denudation rate (reported as a multiple of the upstream rate, "x upstream") is the ratio of downstream to upstream rates. The increase in denudation across the Icacos knickpoint K_{IC} and the Sabana knickpoint K_{SAB} is calculated using data subsets consisting in each case of the trunk channel catchment upstream of each knickpoint, and of the catchments of three downstream tributaries. Due to [10]Be concentration dependency on sediment grain size [Brown et al., 1995, Brocard et al., 2015], results are reported for the coarsest (c: 8–16 mm) and finest (f: 0.75–0.125 mm) measured fractions, as they provide the maximum uncertainty on apparent rates. Results are reported with no correction, then for a suite of cumulative corrections, topographic and vegetation shielding from cosmic rays, effects of the spatial heterogeneity in ground density and soil quartz enrichment, and the effect of time dependence in [10]Be production rate (see Brocard et al. [2015] for details).

Modern [10]Be concentration in river-borne quartz provides estimates of erosion rates, which, in the catchment of Río Blanco, integrate the denudation signal over a few thousands to a few tens of thousands of years [Brocard et al., 2015]. Measured [10]Be concentrations indicate that the knickpoints are still actively retreating today, as evidenced by an increase in catchment-averaged soil erosion rates downstream of the knickpoint lips (Figure 5b and Table 2) [Brocard et al., 2015]. The increase documented by the gravel fraction is slightly larger (*2.1 ± 0.2) than the increase documented by fine sand (*1.7 ± 0.1), where values are expressed as a multiple (*) of the upstream erosion rate. Applying environmental corrections specific to the Luquillo Mountains to these apparent rates [Brocard et al., 2015] tightens the spread to *1.3–1.7 ± 0.1. Such an increase in denudation rate is modest but large enough to radically change the amount of weatherable minerals present in the forest soils [Brocard et al., 2015], and the supply of cations available to vegetation [Porder et al., 2015]. However, such modest increase in denudation may be consistent with the slow knickpoint migration rates suggested by cave dating, in spite of the large differences in the timescale over which both rates are measured. There are, indeed, some potentially complicating factors. First knickpoint propagation may not be steady and may fluctuate over timescales larger than the 4–40 kyr integration time of the detrital [10]Be signal, for example, under the effects of climatic oscillations or of internal oscillations in the coupling between stream incision, slope erosion, and sediment delivery [e.g., Schumm, 1973; Humphrey and Heller, 1995; Frankel et al., 2007]. However, Willenbring et al. [2013] showed that the detrital [10]Be signal can be observed to scale in space and time with the predictions of a numerical model of knickpoint retreat, in a faster eroding setting more sensitive to climatic oscillations. To compare the detrital [10]Be signal to the longer-term pattern of knickpoint propagation, we need to convert the erosion rates into knickpoint celerity. We assume that present-day knickpoint celerity is a function of the difference in average denudation rates above and below the knickpoints, divided by the average slope of the knickpoint faces [Lavé and Avouac, 2001]. This equation assumes that slope downstream of the knickpoint remains constant as the knickpoints migrate upstream (parallel retreat) and does not increase or decrease with upstream migration. In the absence of markers of the downstream change in slope, changes in knickpoint face geometry cannot be addressed. However, this change in slope can be regarded as negligible over the integration time of the [10]Be signal. Due to the dependency of apparent detrital [10]Be erosion rates on sediment grain size in the study area [Brown et al., 1995; Brocard et al., 2015], we calculate knickpoint celerity using the [10]Be concentration measured in two sediment grain sizes (fine (0.75–0.125 mm) and coarse (8–16 mm)), and for different values of soil denudation rates obtained using the measured [10]Be concentrations obtained after applying a series of environmental corrections (Table 3). Using these values of celerity, we then calculate the age at which the knickpoints initiated, assuming first no change in knickpoint celerity with upstream drainage area ($b = 0$ in equation (1) and section 5) and then assuming that celerity scales to the 1/2 power with drainage area, as expected if knickpoint propagation is controlled by unit stream power ($b = 0.5$, discussed further in section 5).

The higher across-knickpoint differential denudation yielded by the coarse sediment fraction provides retreat celerities (0.7–1.0 mm/yr) and initiation ages (2.9–7.8 Myr) consistent with the early Pliocene tilting of the

Table 3. Current Knickpoint Celerity and Projected Time of Initiation of Knickpoint Retreat[a]

Sediment Fraction Considered	Corrections to Detrital Erosion Rate	Inferred Knickpoint Velocity (mm/yr)	b	Age of Knickpoint Intiation (Myr)
Coarse	None	1.01 ± 0.11	0.5	2.9 ± 0.3
			0	5.5 ± 0.6
	All	0.71 ± 0.09	0.5	4.1 ± 0.5
			0	7.8 ± 1.0
Fine	None	0.17 ± 0.02	0.5	17 ± 2
			0	32 ± 3
	All	0.13 ± 0.02	0.5	22 ± 3
			0	29 ± 4

[a]Celerity is calculated using the average increase in detrital ^{10}Be denudation rates across the knickpoints reported in Table 2 (all data set). Conversion to celerity using an average knickpoint face slope of 13% (average of all six knickzones). To capture a wide range of possible estimates, calculations are reported using ^{10}Be values of the coarse (8–16 mm) and fine (0.70–0.125 mm) fractions of stream sediment, applying no correction (None) or the full range (All) of corrections applied to apparent denudations rates in Table 2. Then, ages of knickpoint initiation are calculated assuming either that knickpoint migration is independent of drainage area, a surrogate for stream discharge ($b = 0$, equation (1)), or that knickpoint migration is a function of stream power ($b = 0.5$).

reefal platform and with cave formation at 4.2 ± 0.3 Myr, suggesting that long-term and short-term rates consistently document slow knickpoint migration. The slower apparent velocity yielded by the fine fraction may result from recently reduced differences in the ^{10}Be-constrained denudation rates across the knickpoints due to faster denudation upstream at the timescale of the detrital ^{10}Be record. Some ^{10}Be-based observations upstream of the knickpoint of Río Icacos indeed suggest disequilibrium with faster erosion of hillslopes with respect to hillcrests [*Brown et al.*, 1995], as well as denudation of the topsoil faster than the rate of deepening of the weathering font at the base of the regolith [*Turner et al.*, 2003]. In any case these ^{10}Be-derived retreat rates consistently document slow rates of knickpoint migration along the Río Blanco drainage, which is consistent with the long-term rates of knickpoint migration inferred from cave dating.

5. Processes Governing Slow Knickpoint Retreat

In the following, we explore how stream power, bed load transport, and weathering contribute to the slow migration of these knickpoints, through their effects at various scales. We first compare the current distribution of the knickpoints along the six branches of the Río Blanco drainage with that expected when stream power, bed load fluxes, or weathering dominate (section 5.1). Conclusions drawn from this broad-scale approach regarding the balance between these different processes are then compared and refined using qualitative and semiquantitative field observations of bedrock morphologies along the knickpoint faces (section 5.2).

5.1. Insights From Knickpoint Distribution
5.1.1. Stream Power Dependency
Knickpoint propagation is often thought to be controlled, at least to some extent, by river stream power [e.g., *Miller*, 1991; *Tucker and Whipple*, 2002; *Hayakawa and Matsukura*, 2003, *Bishop et al.*, 2005; *Crosby and Whipple*, 2006; *Willenbring et al.*, 2013]. Nonfluvial processes are thought to be important contributors to knickpoint retreat where knickpoint faces are susceptible to bedrock mass failure, groundwater sapping, or rock weathering [e.g., *Laity and Malin*, 1985; *Baker et al.*, 1990; *Weissel and Seidl*, 1998; *Mackey et al.*, 2014]. Stream power or basal shear stress models are used as simple, convenient proxies for estimating fluvial erosion. In such models, the river-dependent component of knickpoint retreat scales with stream discharge and stream gradient [e.g., *Tucker and Whipple*, 2002; *Bishop et al.*, 2005; *Crosby and Whipple*, 2006]. It is often difficult to evaluate the influence of stream gradient because its temporal evolution is rarely recorded by geomorphologic markers along the knickzones. Some studies suggest, however, that knickpoint retreat is more sensitive to drainage area than to river gradient [e.g., *Bishop et al.*, 2005]. Furthermore, the unit stream power model predicts that knickpoint migration should only depend on drainage area [*Weissel and Seidl*, 1998; *Tucker and Whipple*, 2002]. As such, knickpoint propagation is often simply modeled as:

$$C = \psi A^b \tag{1}$$

where C is the knickpoint lip propagation celerity (m yr^{-1}), A is the drainage area upstream of the knickpoint lip (m^2), ψ is the retreat efficiency (m^{1-2b} yr^{-1}), and b is a nondimensional constant. Drainage area
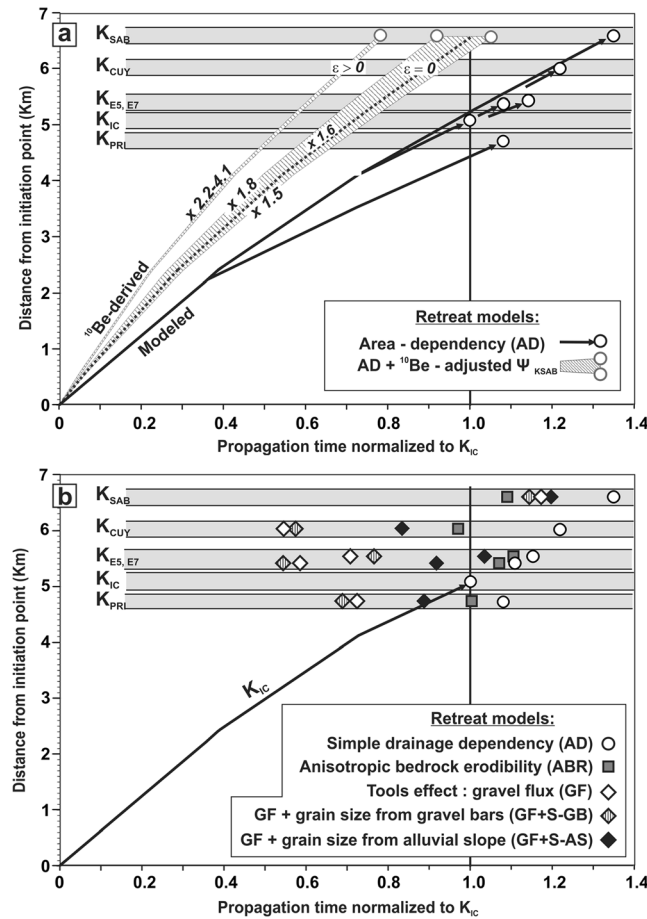
Figure 6. Simulations of knickpoint propagation along the Río Blanco system. Time required for knickpoint lips in the Río Blanco drainage to arrive at their current distance from their initiation point, normalized to the travel time of the Icacos knickpoint K_{IC} (x axis). Displayed knickpoints are those of Río Icacos (K_{IC}), Sabana (K_{SAB}), Cubuy (K_{CUY}), Prieto (K_{PRI}), and of two unnamed streams E5 and E7 (K_{E5} and K_{E7}). (a) Time-distance trajectories and best arrival times for all knickpoints, according to the drainage dependency model (AD, equation (1)). It also shows the trajectory of K_{SAB}, corrected for the difference in retreat celerity between K_{IC} and K_{SAB} derived from the detrital ^{10}Be measurements reported in Table 4 for different cases of upstream erosion (ε; hatched regions). An exact match of arrival times is attained by using a retreat efficiency, ψ, for K_{SAB} that is 1.6 times larger than that of K_{IC} (dotted line). (b) Best fit arrival times of all knickpoints predicted by the drainage area dependency model (AD, equation (1)) to the weathering-controlled model for aniso-tropic bedrock erodibility (ABR, equation (2)), the gravel flux-controlled model (GF, equation (3)), and a grain size-dependent gravel flux model (equation (4)) for two cases: one based on field measurements of bed material on gravel bars (GF + S-GB) and the other based on predicting the bankfull competence from the Shields equation and the local alluvial slope (GF + S-AS) as described in Table 5.

dependency tends to be higher along fast-migrating knickpoints, with $b > 1$ [e.g., *Bishop et al.*, 2005; *Crosby and Whipple*, 2006], than along slowly migrating ones, with $b \leq 0.5$ [e.g., *Weissel and Seidl*, 1998; *Berlin and Anderson*, 2007; *Brocard et al.*, 2012], suggesting that fluvial processes are more effective than other processes at propagating knickpoints. We simulated knickpoint migration along the six major branches of Río Blanco starting at an initiation point defined in section 4.2 (Figure 6a). All catchments have similar elevations and unit discharges even at peak flow [*Pike et al.*, 2010], supporting the use of drainage area as a reasonable proxy for stream power. The fit between modeled and actual knickpoints can be calculated either as the spatial mismatch between the location of modeled and observed knickpoints or as the temporal difference in arrival time of the modeled knickpoint at the location of the observed knickpoints. We hereafter use this latter metric, as it does not require modeling incision beyond the reaches actually incised. Arrival times are normalized to the arrival time of the knickpoint with the largest upstream drainage area (Río Icacos, K_{IC}). Figure 6a shows the best fit simulation for the drainage area-dependent model (AD). The misfit is graphically represented by the scatter of normalized knickpoint arrival times around the vertical line at time = 1.0; a perfect match corresponds to an alignment of all knickpoint arrival times on that vertical line. Normalization is used to explore the influence of drainage area on knickpoint retreat, irrespective of the age of initiation and of the absolute value of retreat efficiency, which here are spatially and temporally constant (area-dependent AD model, Figure 6a). The best fit value of b corresponds to

the minimum standard deviation of knickpoint arrival times. This value, $b = 0.25$, lies halfway between the theoretical value of $b = 0.5$ expected when celerity is controlled by unit stream power and the value $b = 0$ expected when celerity is independent from fluvial erosion (Figure 7a, AD model). Using our estimated age of initiation of 4.2 ± 0.3 Myr, the best fit retreat efficiency is $2.5 \pm 0.2 \cdot 10^{-5}$ m$^{0.5}$ yr^{-1}, about 10 times lower than the retreat efficiency found over steeply bedded shales at similar b values and drainage areas in the subtropical belt [*Brocard et al.*, 2012].
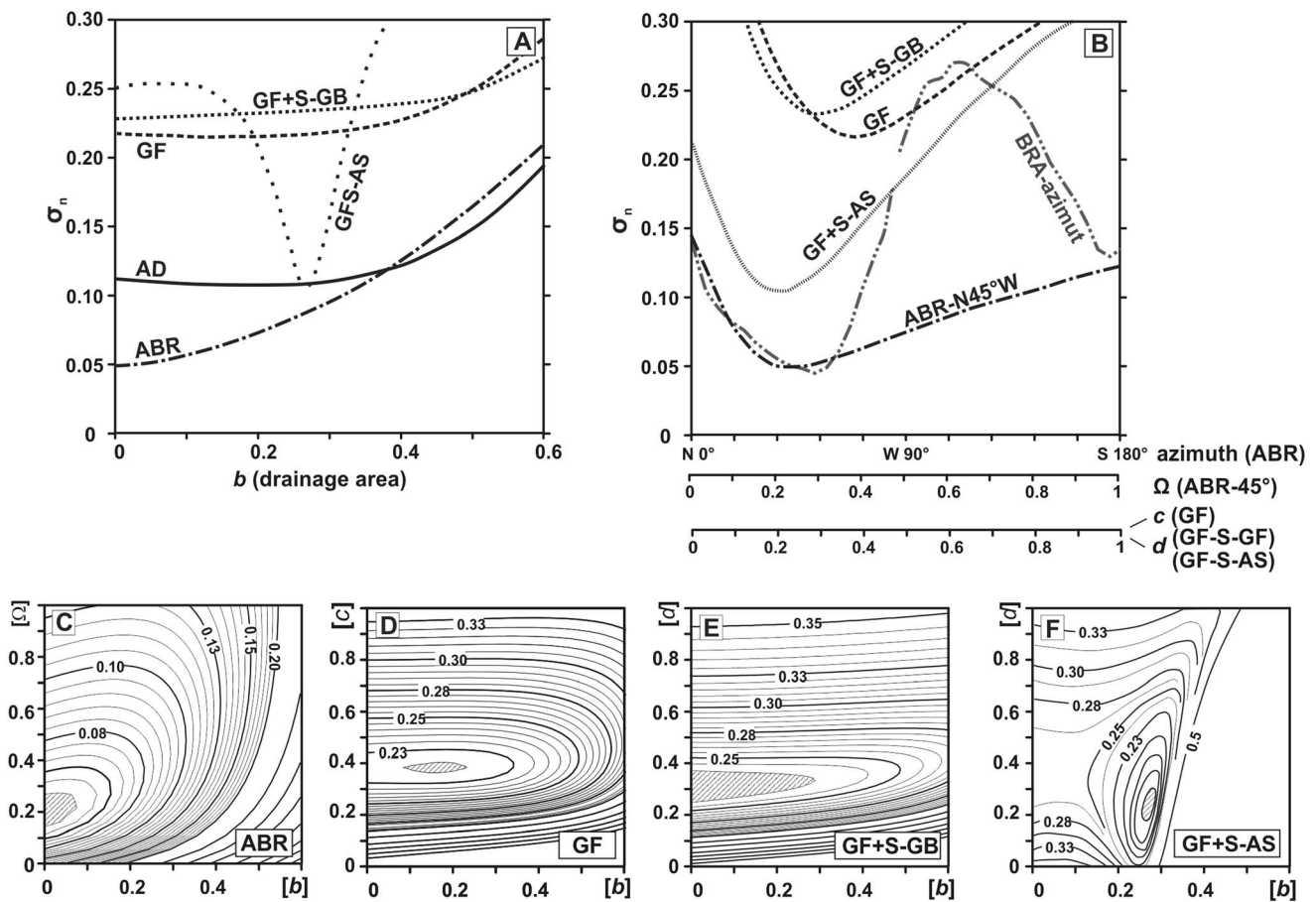
Figure 7. Performance of various simulations of knickpoint migration. (a) Performance of the tested models as a function of the drainage area exponent b, for the simple drainage area model (AD, equation (1)) compared to more complex models, including anisotropic bedrock erodibility (ABR, equation (2)), gravel flux (GF, equation (3)), and grain size-dependent gravel flux (equation (4)) for two cases: grain size measured on gravel bars (GF + S-GB) and the competent grain size at bankfull flow predicted from the Shields equation and the local alluvial slope (GF + S-AS) as described in Table 5. (b) Performance of the tested models as a function of model-specific parameters: bedrock anisotropy (Ω in equation (2)), anisotropy azimuth (°N), and bed load dependency (c and d in equations (3) and (4), respectively). Bottom panels show contour plots of σ_n as a function of drainage area-dependent erosional processes (b exponent in equation (1)), and as a function of (c) bedrock anisotropy (Ω in equation (2)), (d) bed load flux (c exponent in equation (3)), and (e and f) grain size-dependent bed load flux (d exponent in equation (4)) for the two cases described above: (GF + S-GB) and (GF + S-AS), respectively. Hatched regions indicate σ_n minima and, thus, the best fit values. Note the finer contour intervals in Figure 7c.

5.1.2. Unevenness in Retreat Efficiency According to Detrital [10]Be Erosion Rates

The simple drainage area-dependent model (AD, equation (1)) predicts that K_{IC} reaches its current location before other knickpoints reach their respective locations, all other knickpoints arriving at their current location at times $> 1 \; T_{IC}$ (AD model, Figures 6a and 6b). In other words, once weighted for the effect of drainage area, branch IC is shorter than, for example, branches SAB and CUY. For this reason K_{IC} also lies at a distinctly shorter χ distance on a χ plot (Figure 3, inset), as χ is a measure of upstream distance weighted by drainage area [*Perron and Royden*, 2012].

The amount of deviation from a simple area-dependent model is consistent with differences in [10]Be-derived increases in soil denudation rate measured across knickpoints K_{IC} and K_{SAB}. In section 4.2, a general [10]Be retreat rate was obtained by contrasting the means of all [10]Be-derived denudation rates measured upstream and downstream of the knickpoints. This average rate was found to be consistent with retreat rates integrated over millions of years. These measurements can be analyzed in greater detail to contrast [10]Be-derived erosion rates across K_{SAB} and K_{IC} (Table 4). The downstream increase in denudation rate of K_{SAB} is found to be 10–40% larger than downstream of K_{IC}. Conversion of denudation rate to knickpoint celerity (section 4.2) then predicts that K_{SAB} propagates 1.5–1.8 times to 2.2–4.1 times faster than K_{IC}, K_{IC} being 32% steeper than K_{SAB} (Figure 6a, hatched areas). The difference in the current location of K_{SAB} and K_{IC} can be reproduced

Table 4. Differential Retreat Celerity of K_{SAB} With Respect To K_{IC}, As Documented by Detrital ^{10}Be Erosion Rates[a]

Sediment Fraction	Corrections to ε^{10}Be Rate	ε ^{10}Be Rate (x Icacos)	C_{SAB} for $\varepsilon = 0$ Above Knickpoint (x Icacos)	C_{SAB} for $\varepsilon > 0$ Above Knickpoint (x Icacos)
Coarse	None	1.12	1.48	2.19
	All	1.11	1.47	2.24
Fine	None	1.36	1.80	2.22
	All	1.32	1.75	4.06

[a]Due to the dependency of the detrital ^{10}Be concentration on sediment grain size (coarse (8–16 mm) versus fine (0.70–0.125 mm) fractions), and the effects of environmental corrections on erosion rate estimates [*Brocard et al.*, 2015], the table presents various calculations of the differential retreat efficiency of K_{SAB} with respect to K_{IC}, expressed as a multiple (x) of the celerity of K_{IC}. The calculations capture the widest possible range of differences in celerity between the Icacos (K_{IC}) and Sabana (K_{SAB}) knickpoints. We suspect a recent increase in erosion upstream of the knickpoints (see section 4.2), and therefore, we evaluate the maximum effect of such an increase on the differential migration of both knickpoints by calculating the differences using two end-members as a sensitivity analysis, with a case with no upstream erosion ($\varepsilon = 0$) and another end-member that assumes upstream erosion equal to the measured ^{10}Be average ($\varepsilon > 0$).

through modeling by ascribing K_{SAB} a retreat efficiency ψ 1.6 times larger than that of K_{IC} (Figure 6a, dotted line). This difference is remarkably similar to the predictions of the ^{10}Be signal, considering the differing time-scales of integration and the simplicity of the conversion model. The concordance of these approaches suggests that departures from the simple drainage area model may correspond to differing characteristics in these knickpoints. We identified two notable differences between these knickpoints: their overall propagation direction with respect to prevailing bedrock anisotropy and drastic differences in the bed load size and fluxes at the knickpoint lips. These differences facilitate a better understanding of the mechanisms that drive knickpoint retreat along the Río Blanco, as discussed below.

5.1.3. Effects of Variations in Bedrock Erodibility

The Río Blanco quartz diorite is a coarse-grained crystalline rock of homogenous composition, containing abundant, but widely interspersed decametric enclaves of diorite. Analysis of jointing along the knickzones (Figure 8) indicates that typically, jointing includes three prevalent mutually perpendicular sets of joints, two vertical ones and a horizontal one (Figure 8). These joints typically display a regular 1 to 2 m wide spacing (Figures 9c and 9e). In places, additional, moderately dipping sets are well expressed, as well as occasional left-lateral strike-slip faults. Water flow is often controlled by jointing at the meter to decameter scale, the flow direction being generally controlled by three dominant sets, which generally include two orthogonal subvertical sets and a shallow-dipping one. At places only one set is well expressed, in which case water flows alternatively unconstrained, over massive exfoliating bedrock, and channeled into joint-controlled slots. At a larger scale, this strong local control of jointing on water flow has little effect on the general shape of the Río Blanco drainage, which is essentially dendritic. However, the branches that are subparallel to the well-expressed NW-SE joint set have experienced the largest amount of knickpoint migration (K_{SAB} and K_{CUY}, Figure 8), and as a result, the incised drainage seems to have expanded dominantly in the NW-SE direction. Since the basic model of drainage area dependency underestimates the celerity of K_{SAB} and K_{CUY} with respect to K_{IC}, we explored the possibility that migration has been faster in a NW-SE direction due the greater erodibility and/or faster weathering along NW-SE oriented joints. We introduced an anisotropy factor Ω which is the ratio of the retreat efficiency in a direction perpendicular to the direction of the dominant joint set to the retreat efficiency parallel to the dominant joint set, projected onto the direction of flow over length increments of 5 m.

$$C = \psi^\circ \Omega A^b \qquad (2)$$

where ψ° is an effective retreat efficiency that encapsulates the effects of weathering and jointing on bedrock erodibility with respect to discharge-dependent erosion processes. We refer to equation (2) as the anisotropic bedrock erosion model (ABR). As in previous simulations, we searched for the best fit between modeled and observed knickpoint locations, still defined as the lowest standard deviation of knickpoint arrival times at their present location (ABR, Figure 6b). The search for the best fit value was conducted by concurrently varying b between 0 and 1, the anisotropy azimuth over 180° (ABR-azimuth, Figure 7b), and Ω between 0 and 1 (illustrated for the best fit azimuth value of N45°W, Figure 7b). Adding bedrock anisotropy significantly improves the fit compared to the isotropic model for low values of b (ABR versus AD, Figure 7a) and particularly in the absence of influence of drainage area ($b = 0$, Figures 7a and 7c). In this case the anisotropic model
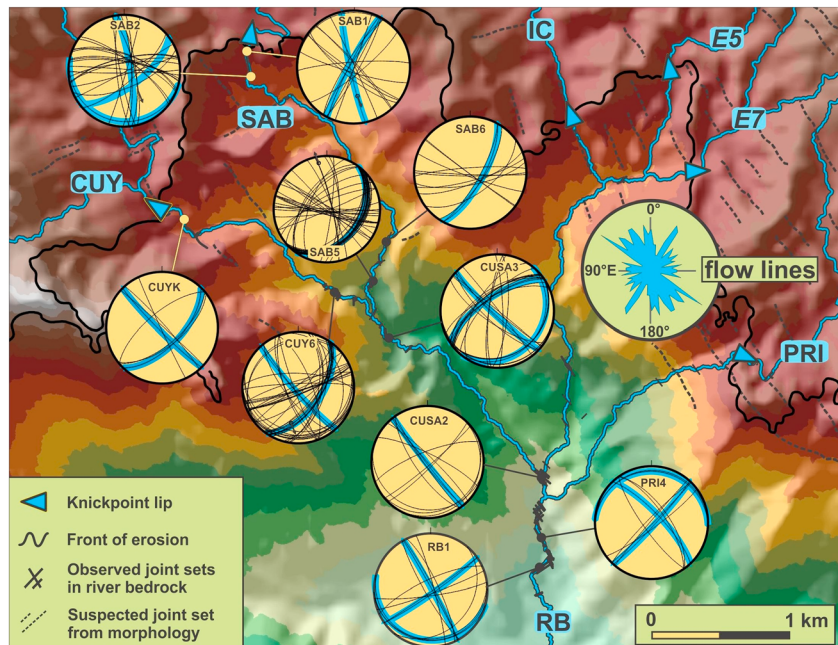
Figure 8. Joint orientations along Río Blanco, projected onto lower hemisphere Wulf stereoplots using software WinTensor 5.0.7 [*Delvaux and Sperner*, 2003]. Blue lines: planes followed by water flow at these same sites. Above the knickpoint lips, bedrock does not crop out and the fabric is inferred from topographic lineaments. The rose diagram shows the statistical orientation of flow lines along all 50 m long reaches within the incised drainage network. It illustrates the tendency of the incised drainage to develop in a NW-SE direction.

performs better than the isotropic model for joint orientations between N10°W and N140°, the best fit being obtained at N45°W. Best fit values are obtained for an isotropy such that retreat efficiencies are 1.25 to 10 times greater in the direction of jointing than in a direction perpendicular to jointing (ABR: 45°W, Figure 7b), the best fit being attained for a retreat efficiency 5 times greater ($\Omega = 0.2$). Examination of the spread in arrival times (ABR, Figure 6b) shows that the anisotropic bedrock model reduces misfit along all branches. A model where retreat is controlled by variations in bedrock erodibility therefore more closely reproduces the observed distribution of knickpoint lips than the simple drainage area model (a surrogate for shear stress or stream power).

5.1.4. Effect of Bed Load Abrasion ("Tools" Effect)

Among the tributaries of Río Blanco, Río Icacos stands out for its headwaters draining almost exclusively quartz diorite (Figure 5b). Quartz diorite weathers to a sandy saprolite that contains residual corestones several meters across [*Brantley et al.*, 2011]. Upon arriving at the surface, the saprolite erodes to sand and clays. As a result, the streams that only drain quartz diorite have very shallow gradients (Figure 3) and have sandy bed load (Figure 9a). For this reason Río Icacos carries little gravel down to its knickpoint [*Pike et al.*, 2010] (Table 5). The aureole of volcanoclastic hornfels that surround the quartz diorite delivers more volcanoclastic gravel into the other tributaries of Río Blanco. As a result, and in spite of receiving sandy tributaries while crossing the diorite, the other branches of Río Blanco are more steeply graded (Figure 3) and carry gravel down to their knickpoint lips (Figure 9b and Table 5). *Pike et al.* [2010] showed that sediment transport capacity along the knickzones is much larger than the threshold for sediment mobility, implying that gravel is rapidly conveyed downstream while sand is flushed in suspension. Small particles in suspension tend to cause less erosion than gravel saltation [e.g., *Sklar and Dietrich*, 2001; *Lamb et al.*, 2008]. Because of this high transport capacity, an increase in the flux of bed load particles is expected to increase the rate of abrasion ("tools effect"), while protection of the bedrock by stationary gravels over the bedrock should remain minimal ("cover effect" [*Sklar and Dietrich*, 1998]). At such high capacity, abrasion should also increase with increasing bed load grain size [*Foley*, 1980; *Turowski et al.*, 2015], resulting in a positive scaling between sediment flux, bed load grain size, and knickpoint celerity. Bed load fluxes have been found to play an important role in accelerating knickpoint celerity [e.g., *Jansen et al.*, 2011; *Cook et al.*, 2013].
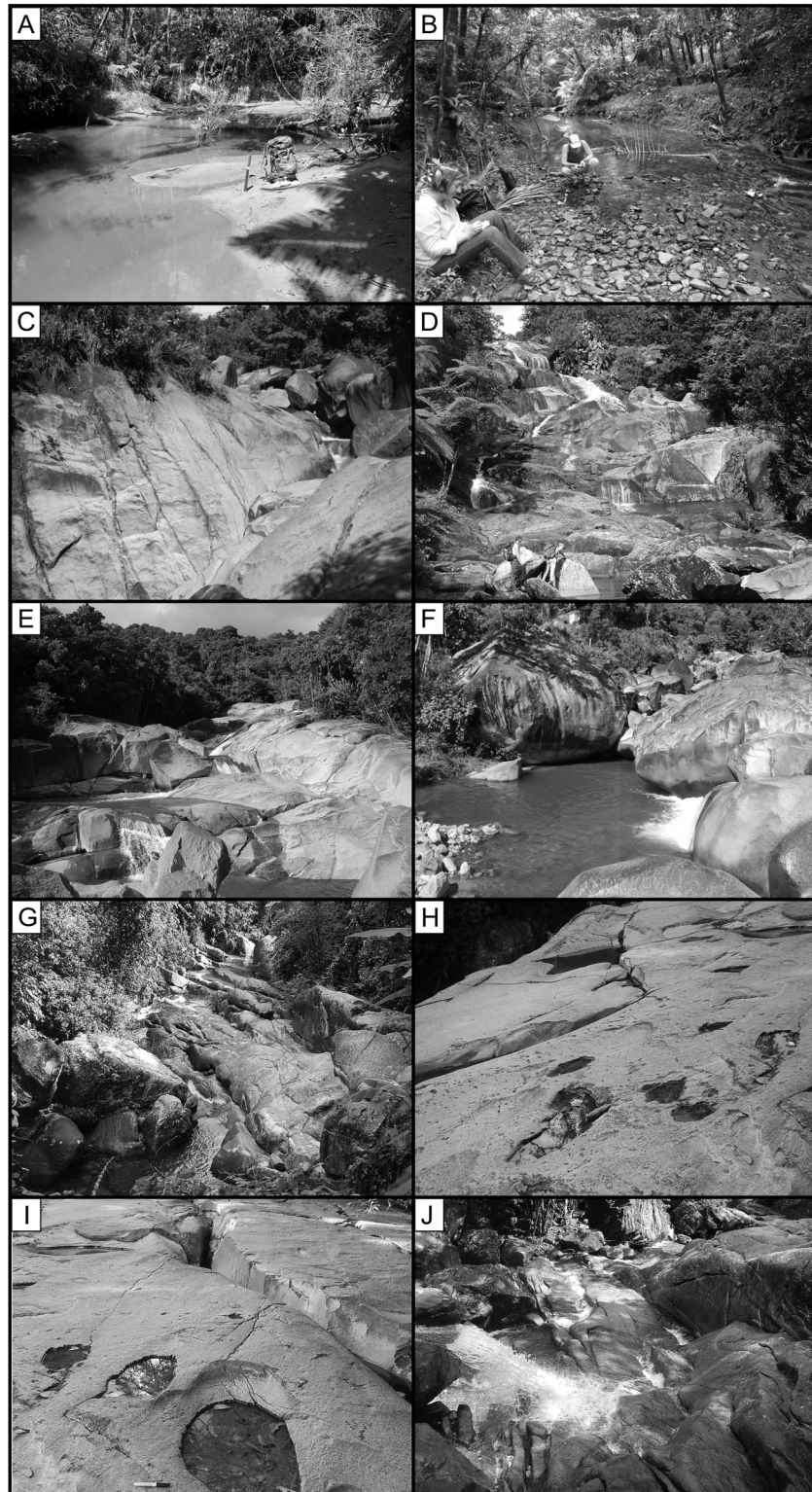
Figure 9. Field views of knickpoints (see Figure 5 for location). (a) Sandy river above knickpoint (Icacos), (b) gravelly river above knickpoint (Sabana), (c) joint spacing in quartz diorite, (d) typical waterfall face, (e) boulder-free reach, (f) top weathering and side abrasion on quartz diorite corestone and transiting gravel, (g) sediment-starved reach, (h) weathering ponds (gnammas) in shallow scallops, (i) vertical weathering in joint next to weathering ponds, and (j) morphology of quartz diorite weathering in active river bed.

Table 5. Geometric Characteristics Used to Model the Influence of the Tools Effect on Knickpoint Retreat

Knickpoint Name	Knickzone Gradient (%)	Knickzone Steepness[a]	Upstream Gradient (%)	Upstream Steepness[a]	Regional D_{50}[b] (cm)	Field D_{50}[c] (cm)	Upstream Area (km^2)	Gravel-Feeding Area[e] (%)
IC	15.0	2.58	0.9	1.26	3	$4_{[1-9]}/0.3_{[0-1]}$[d]	4.16	0.3
SAB	10.5	2.35	2.1	1.57	12	$8_{[3-29]}$	3.08	7
CUY	13.5	2.43	3.5	1.79	28	$28_{[1-10]}$	3.15	47
PRI	27.0	2.62	2.7	1.54	19	$8_{[1-12]}$	1.66	24
E5	12.1	2.10	3.8	1.39	19	$18_{[1-2]}$	0.36	3
E7	11.9	2.20	3.7	1.66	25	$7_{[1-13]}$	1.30	19

[a]Normalized steepness K_{sn} [*Tucker and Whipple*, 2002] defined over 500 m upstream and downstream of the knickpoint lip for $K_{sn} = A^{0.5}S$, where S is the slope and A the drainage area in km^2.
[b]Median bed surface grain size D_{50} is estimated using drainage area A, upstream stream gradient S, and a series of functional relationships: grain size predicted in terms of the bankfull competence using the Shields equation, $D_{50} = \tau/(\tau*_c g(\rho_s - \rho_w))$, where τ is the bankfull shear stress, $\tau*_c$ is the critical Shields parameter (set equal to 0.050), g is gravitational acceleration, and ρ_s and ρ_w are sediment and water densities (2700 and 1000 kg m^{-3}), respectively. The reach-average shear stress is $\tau = \rho_w gSR$, where S is the local channel slope and R is the hydraulic radius for a rectangular channel, $R = wd/(w + 2d)$, where w is channel width and d is flow depth. The latter two are predicted from downstream hydraulic geometry relations developed by *Pike et al.* [2010], $w = 5.4Q_{bf}^{0.33}$ and $d = 0.6Q_{bf}^{0.12}$. In these relations, the bankfull discharge (Q_{bf}) is determined as $Q_{bf} = A(0.0042 E_{avg} + 0.406)$, where E_{avg} is the average elevation of the upstream catchment.
[c]Grain size measured in the field on gravel bars displaying evidence of recent mobility. Numbers in brackets refer to the number of manual counting sites followed by the number of photo sieving sites.
[d]Median bed load grain size along the sandy Icacos River.
[e]Feeding area expressed as a fraction of the total feeding area of Río Blanco.

We tested the ability of the tools effect to account for the amount of knickpoint migration by modulating knickpoint celerity by bed load flux

$$C \simeq \psi' \, A^b F^c \tag{3}$$

where F is the bed load feeding area composed of volcanoclastic substrate (m^2, Table 5), A the total upstream drainage area (m^2, Table 5), and ψ' and c parameters encapsulating the effects of bed load flux on celerity. We refer to equation (3) as the gravel flux model (GF). Best fit solutions to parameters b and c (Figure 7d) suggest again a weak dependency on drainage area ($b < 0.3$), and a moderate dependency on gravel flux ($c = 0.4$). Including bed load fluxes effectively accelerates all knickpoints with respect to K_{IC} (GF versus AD, Figure 6b). However, knickpoint retreat is overaccelerated in rivers with abundant gravel, causing overall poor performance compared to the simple-area-dependent model (GF versus AD, Figures 7a and 7b). An alternative formulation was therefore implemented to take into account the effect of bed load grain size

$$C \simeq \psi'' \, A^b (F \, D_{50})^d \tag{4}$$

where D_{50} represents the median grain size and ψ'' and d parameters encapsulate the combined effects of bed load flux and grain size on celerity. D_{50} was assessed in two ways, first through direct field measurements of the gravel size on bars immediately upstream of the knickpoint lips (Table 5, model GF + S-GB, Figure 6b) and second, based on a prediction of the bankfull competence using the Shields equation, local slope, and hydraulic geometry relationships developed by *Pike et al.* [2010] from 234 sites in the Luquillo Mountains, including the Río Blanco drainage (Table 5, model GF + S-AS, Figure 6b). Though less precise than direct field measurements, this calibration over many streams is less sensitive to potential short-term fluctuations in bed material grain size that could bias one-time measurements on the gravel bars. Adding the contribution of the sand fraction approximated by the extent of the quartz diorite feeding area has negligible effect on the output due to the very small median size of the sandy streams (Table 5). Because gravel only stems from the headwaters, bed load grain size is expected to decrease in the downstream direction, and the distance from the feeding area might have to be taken into account. In fact, this effect can be neglected because the distance between the feeding areas and the knickpoints remains short compared to the characteristic length of gravel comminution in the Luquillo Mountains [*Miller et al.*, 2014]. Both estimations of D_{50} (derived from bed material measurement on gravel bars and estimated from the bankfull competence using the local stream slope) agree in four out of the six streams, while measured D_{50} is much lower along two of the six streams. This discrepancy may arise from the fact that along these streams, gradient is set by a population of distinctly coarser, less mobile volcanoclastic boulders, while field measurements targeted more mobile gravel bar material. The model calibrated to bankfull competence using the local alluvial slope to infer grain

size upstream of the knickpoint lips (GF + S-AS, Figure 6b) performs better than the model calibrated using field measurements of mobile gravel bars, with residuals twice as small (GF + S-AS versus GF + S-GB, Figures 7a and 7b). Both perform better than the simple bed load flux model (GF, Figures 7a and 7b). They do not perform better than the simple drainage area-dependent model (AD, Figures 7a and 7b) but yield knickpoint arrival times distributed more evenly around that of K_{IC} (Figure 6b). Best fit values in either case again indicate a weak dependency on drainage area ($b \leq 0.25$, Figures 7d–7f).

The exploration of the knickpoint distribution therefore suggests that, overall, knickpoint propagation weakly correlates to stream discharge ($b = 0$–0.3, according to inspection of Figures 7a and 7c–7f). Incorporating bed load fluxes and grain size strongly modifies the predicted temporal distribution of the knickpoints (Figure 6b) and produces variations in knickpoint celerity that mirror modern variations in knickpoint celerity deduced from the spatial variability in detrital [10]Be soil erosion rates. These "tool" models still predict a poor dependency of knickpoint celerity on stream discharge. A model taking into account the influence of bedrock jointing on knickpoint retreat yields the best fit to the observed distribution. The modeling consistently documents a weak dependency of knickpoint retreat on stream discharge and leaves open questions regarding the dominant processes, which we investigate below using field observations. In order to identify the processes at work along the knickzones, we review the marks left by these different processes on streambed morphologies and evaluate their compatibility with the conclusions drawn from knickpoint distribution in the following section. The field observations only show the processes at work today, while the modeling provides a deeper perspective on how such processes may have shaped the incised network over time.

5.2. Field Observations on the Relative Efficacy of Plucking, Abrasion, Weathering, and Mass Wasting

An observation of riverbed morphology along the knickpoint faces provides important insights on the respective contribution of plucking, abrasion, weathering, and mass wasting [e.g., *Wohl*, 1998; *Montgomery*, 2004; *Richardson and Carling*, 2005]. The knickzones are composed of an alternation of bare bedrock and boulder-strewn reaches (Figure 5a). The boulders are corestones unearthed from the surrounding slopes; they slide or creep downslope and end up in the river channel. There, the location of weathering and abrasion features at their surface indicates that they remain mostly immobile and decay in place through a combination of chemical weathering at their top and abrasion around their base (Figure 9f) until underlying bedrock becomes reexposed. Bedrock incision is usually achieved through a combination of plucking and abrasion [e.g., *Whipple et al.*, 2000]. Field observations indicate that joints typically display a 1 to 2 m wide spacing (Figure 9c). Fresh surfaces left by plucking are rarely observed in the field and are only seen at a few particular places characterized by unusual decimeter-scale joint spacing. Qualitative observations thus suggest that plucking along the knickzones is rare. Bed forms typically produced by abrasion, such as scallops and potholes [*Richardson and Carling*, 2005], are equally rare. Potholes were observed at only one place. Scallops are more common; they are, however, very shallow and are floored by weathering hollows (gnammas) where water can pond in the scallops (Figure 9h). The irregular outline of the gnammas is hardly modified by subsequent abrasion, indicating that abrasion rate is outpaced by weathering rate. Weathering features, such as blunt edges left after spallation of rindlets are observed along vertical joints in the streambeds, even on the floor of active channels (Figures 9i and 9j). These observations suggest that bed load-driven abrasion is very slow along the knickzones. This can happen if the bedrock is shielded from abrasion beneath a sediment cover (cover effect [*Sklar and Dietrich*, 2006]) or, on the contrary, if the bed load flux is limited [*Sklar and Dietrich*, 2006]. Bed load storage along the knickzones in the form of fill terraces and gravel bars is close to nonexistent. Very little gravel is found trapped in plunge pools, bedrock clefts, or between boulders (Figures 9e–9g). All of these observations imply that the streams are essentially sediment starved.

The scarcity of plucking and abrasion morphologies and the widespread preservation of weathering features indicate that plucking and abrasion operate very slowly and, at most at the pace of geochemical weathering. The weathering rate of the quartz diorite under soil cover is well quantified upstream of the knickpoints, where saprolite basal propagation rates of 58 to 87 m Myr^{-1} have been inferred from weathering balances and dissolved exports [*White et al.*, 1998; *Stallard*, 2012]. Deepening rates of the saprolite/bedrock interface of 45 m Myr^{-1} have been obtained using U-series nuclides [*Chabaux et al.*, 2013]. These values may represent an upper bound for the weathering rate of barren rock along the knickpoint faces, because barren rock typically weathers more slowly than soil-mantled rock. Limited plucking and abrasion is also consistent with the slow knickpoint celerity inferred from catchment-averaged [10]Be erosion rates of 70–180 m Myr^{-1} along the

knickpoint faces [*Brocard et al.*, 2015], and with knickpoint integrated celerities of a few millimeters per year over the past 4.3 Myr (section 4.2). The weak dependency of retreat rates on drainage area (section 5.1) further suggests that these stream power-dependent processes are slow enough for nondischarge-dependent processes to take over and control knickpoint retreat rates. In particular, limited plucking and abrasion by bed load particles could explain the poor performance of the simple drainage area and bed load flux models, respectively.

Field observations suggest that in the absence of other competing processes, bedrock eventually yields through the opening of vertical joints by a combination of chemical weathering and scouring (Figures 9i and 9j). The continued enlargement of such fractures leads to the isolation of large bedrock slabs that topple or slide away. The higher erodibility in the NW-SE direction does not seem to result from a higher density of NW-SE trending joints, but rather from an intrinsic weakness of these joints to weathering and erosion. They may have experienced cataclasic shearing during Eocene time, when large, N70°W left-lateral faults developed throughout Puerto Rico [*Jolly et al.*, 1998]. Along the most massive bedrock reaches, exfoliation of slabs a few decimeters thick prevails. It seems therefore that the pace of bedrock removal and knickpoint migration is set by a combination of weathering along bedrock joints, exfoliation, and by the eventual gravitational removal of large blocks which could occur at high flow but could also be triggered by other events such as earthquakes or by the landing of landslides stemming from the surrounding slopes. This combination of processes together may weakly correlate with stream power. The above observations are consistent with the best fit model for knickpoint retreat being one in which erodibility is greatest along a NW-SE oriented set of fractures. The importance of weathering on the pace of river incision is probably underappreciated but is increasingly recognized, especially for sedimentary bedrock [*Montgomery*, 2004]. The bed forms found along the knickpoints of the Río Blanco drainage suggest that weathering can also significantly contribute to river incision on plutonic bedrock.

6. From Processes to Rates: The Persistence of Upland Relict Landscapes

In the Luquillo Mountains, the dramatic knickpoints described here are only observed along rivers that drain quartz diorite. The rivers that drain the surrounding volcanic and volcanoclastic terrain display either fully relaxed concave up profiles, disrupted by minor knickpoints that coincide with massive layers, or more irregular profiles with diffuse knickzones, which represent either subdued waves of incision, or broad-scale adaptations to changes in bedrock erodibility (see supporting information Figure S2-2). The quartz diorite therefore exerts a first-order control on the development rate and/or preservation of migrating knickpoints. The bedrock control acts in two ways: first, it slows down headward knickpoint migration, such that the wave of incision is still seen today migrating up the Río Blanco drainage, several million years after its initiation; second, the quartz diorite favors the preservation of steep knickpoint faces. Retreat of the knickpoint faces is slow because the usual processes of bedrock erosion, plucking and abrasion, are relatively ineffective along the knickzones. Plucking is frequent on the highly fractured and thinly bedded volcanoclastic rocks [*Pike et al.*, 2010] but is infrequent on the quartz diorite due to the wide spacing of the joint sets. Abrasion is rendered inefficient through a combination of factors upstream of the knickpoints: a wide occurrence of the quartz diorite and a protective vegetation cover. In the rainforest, soils contain abundant and well-connected macropores that efficiently convey runoff underground as quick flow [*Beven and Germann*, 1982] and reduce overland flow to a fraction of a percent, even during the most intense rain showers [*Larsen et al.*, 1999; *Harden and Cruggs*, 2003; *Schellekens et al.*, 2004; *Larsen et al.*, 2012]; they also prevent pore pressure buildup, reducing landslide frequency [*Simon et al.*, 1990]. As a result, over the quartz diorite, denudation rates are low for such a steep tropical mountain, only reaching of a few tens of meters per million years [*Brown et al.*, 1995; *Brocard et al.*, 2015]. Coeval high weathering rates [*White et al.*, 1998; *Turner et al.*, 2003; *Chabaux et al.*, 2013] have resulted in the development of a thick saprolite [*Brantley et al.*, 2011; *Buss et al.*, 2013]. Erosion of the saprolite feeds streambeds with a bimodal population of corestones several meters across and sand. While corestones decay in place, the stream feeds knickpoints with sand, which has little abrasive power. Volcanoclastic rocks weather to a clayey saprolite and boulder-to-pebble-sized blocks. While saprolite gravels soon disintegrate [*Miller et al.*, 2014], a small fraction of nonweathered gravel makes it way to the knickpoint lips and contributes to erosion along the knickzones. However, due to the low erosion rates and intense weathering upstream, this overall flux of gravel is small, and streams are gravel-starved along the knickpoint faces.

The low activity of stream power-dependent erosion processes leads to a dominance of weathering and mass wasting along the knickpoint faces, in a way similar to what is observed along vertical knickpoints [*Laity and Malin*, 1985; *Baker et al.*, 1990; *Weissel and Seidl*, 1998; *Crosby and Whipple*, 2006; *Mackey et al.*, 2014]. This is evidenced by the weakness of the dependency of knickpoint celerity on drainage area, and by the apparent sensitivity of knickpoint retreat to joint orientation in the quartz diorite. Weathering along bedrock joints, exfoliation, and toppling of large blocks becomes the process that sets the rate of knickpoint retreat. As weathering and toppling become the limiting factors of knickpoint retreat, the maintenance of steep knickpoint faces becomes necessary for retreat to proceed. The fact that the Icacos River knickpoint has the steepest face among the knickpoints developed only into the quartz diorite (Table 3) can then be explained by its sandy bed load, which ensures a complete predominance of nonfluvial processes.

Geomorphologists have differentiated weathering-limited and transport-limited landscapes [*Carson and Kirby*, 1972]. In the former, the rate of formation of erodible debris by physical and chemical processes controls the rate of landscape lowering [e.g., *Baldwin et al.*, 2003; *Sklar and Dietrich*, 2006]. The relict landscape of the Luquillo Mountains, with its deep regolith, is transport limited, while the knickzones are clearly weathering limited, but this latter characteristic is inherited from the upstream properties of the relict landscape. In essence, by starving the knickpoints from erosion tools, the relict landscape slows knickpoint progression, effectively protecting itself from dissection. The specific contribution of the quartz diorite is to reduce plucking along the knickpoint face and to weather to a saprolite that erodes to sand and scarce gravel over the relict landscape. Over the volcaniclastic landscape, knickpoints have largely migrated and diffused, presumably because the bedrock is more densely fractured and thus more prone to plucking, while abrasion is favored by a saprolite that contains gravel-sized material which release more bed load to the streams.

Shore platforms are still largely preserved all over the island of Puerto Rico. Their preservation can be explained by the overall lower slopes of the shore platforms (14.4°) compared to the steeper relict island of El Yunque. The platforms are blanketed by the most deeply evolved soils of the island [*Beinroth*, 1982], and we hypothesize that they similarly deliver little bed load to the head of the canyons that are currently propagating through them. Bed load starvation could likewise explain the extensive preservation of upland relict landscapes in many mountain belts. Depending of the location, it would result from sediment flux limitations due to factors such as subdued slopes, effective protection of soils by vegetation, advanced weathering of the relict landscape, and bedrock prone to weathering but resistant to stream erosion.

7. Conclusions

Rivers along the southern flank of the Luquillo Mountains drain a massive stock of quartz diorite. Over this homogenous substrate rivers have developed prominent knickzones, the lips of which cluster about the 600 m elevation of a long-known low-relief surface that surrounds the Luquillo Mountains. We interpret this surface as a former shore platform that has formed and has been uplifted after the early Pliocene (5 Myr ago). Knickpoints in the Río Blanco drainage have developed following the uplift of this platform and are since retreating toward the headwaters of the drainage.

Previous investigation of these knickpoints using detrital ^{10}Be in river-borne quartz had shown that passage of these topographically dramatic knickpoints is associated with a modest, twofold increase in denudation [*Brocard et al.*, 2015]. Here using ^{10}Be-^{26}Al dating of caves that have formed following the emergence of the shore platform, we find that knickpoints initiated 4.2 ± 0.3 Myr and have retreated only 5–7 km since. Using a simple model for converting modern detrital ^{10}Be denudation rates into knickpoint celerity we show that both independent datasets are consistent and point to a very slow rate of knickpoint propagation.

Variations in knickpoint retreat rate deduced from spatial variation in detrital ^{10}Be denudation rates are consistent with the current distribution of the knickpoints. Knickpoint retreat along each of the different branches of the Río Blanco drainage is not well described by a simple drainage area (stream power) model nor do models that incorporate the effects of bed load flux (abrasive tools) and the size of bed material perform much better. A model that incorporates the effect of bedrock weathering along vertical joints produces the best fit to the current knickpoint distribution. All models point to a weak dependency of knickpoint retreat on drainage area.

Inspection of the knickpoint faces confirms the inferences from the knickpoint distribution, revealing a weak contribution of abrasion and plucking to knickpoint retreat. Weathering and exfoliation are largely developed and seem to set the pace of knickpoint retreat.

Slow rates of erosion upstream of the knickpoints limit the delivery of bed load to the knickpoint lips, thereby limiting abrasion. The effect is reinforced by the nature of the quartz diorite, which weathers to sand, providing little abrasion tools, while in the meantime constituting a bedrock very resistant to plucking. In the Luquillo Mountains, steeper topography is not correlated with increased erosion due to a very efficient limitation of surface denudation by the native vegetation cover. At the scale of Puerto Rico, however, as in other mountain ranges, the preservation of large expanses of shore platforms could be mostly due to limited bed load fluxes and reduced sediment grain sizes out of the flattest regions of the topography, where erosion rates are generally low and weathering much more advanced than in the steeper portions of the landscape.

References

Anderson, R. S. (2002), Modeling the tor-dotted crests, bedrock edges, and parabolic profiles of high alpine surfaces of the Wind River Range, Wyoming, *Geomorphology*, *46*, 35–58.

Babault, J., J. van Den Driessche, S. Bonnet, S. Castelltort, and A. Crave (2005), Origin of the highly elevated Pyrenean peneplain, *Tectonics*, *24*(2), doi:10.1029/2004TC001697.

Baker, V. R., R. C. Kochel, J. E. Laity, and A. D. Howard (1990), Spring sapping and valley network development, *Geol. Soc. Am. Spec. Pap.*, *252*, 235–265.

Balco, G. (2009), ^{26}Al-^{10}Be exposure age/erosion rate calculators: Update from v. 2.1 to v. 2.2, CRONUS Online Calculator. [Available at http://hess.ess.washington.edu.]

Balco, G., J. O. Stone, N. A. Lifton, and T. J. Dunai (2008), A complete and easily accessible means of calculating surface exposure ages or erosion rates from ^{10}Be and ^{26}Al measurements, *Guat. Geochron.*, *3*, 174–195.

Baldwin, J. A., K. X. Whipple, and G. E. Tucker (2003), Implications of the shear stress river incision model for the timescale of post-orogenic decay of topography. *J. Geophys. Res.*, *108*(B3), 2158, doi:10.1029/2001JB000550.

Beinroth, F. H. (1982), Some highly weathered soils of Puerto Rico: 1—Morphology, formation, classification, *Geoderma*, *27*, 1–73.

Berlin, M. M., and R. S. Anderson (2007), Modeling of knickpoint retreat on the Roan Plateau, western Colorado, *J. Geophys. Res.*, *112*, F03S06, doi:10.1029/2006JF000553.

Beven, K., and P. Germann (1982), Macropores and water flow in soils, *Water Resour. Res.*, *18*(5), 1311–1325.

Bishop, P., T. B. Hoey, J. D. Jansen, and I. Lexartza-Artza (2005), Knickpoint recession rate and catchment area: The case of uplifted rivers in Eastern Scotland, *Earth Surf. Processes Landforms*, *30*(6), 767–778, doi:10.1002/esp.1191.

Brantley, S. L., H. Buss, M. Lebedeva, R. C. Fletcher, and L. Ma (2011), Investigating the complex interface where bedrock transforms to regolith, *App. Geochem.*, *26*, 12–15.

Briggs, R. P. (1966), The blanket sands of northern Puerto Rico, presented at the 3rd Caribbean Geol. Conf., Kingston, Jamaica, 1962, Trans. Jamaica Geol. Surv. Publ. *95*, 60–69.

Briggs, R. P., and E. Aguilar-Cortés (1980), Geologic map of the Fajardo and Cayo Icacos quadrangles, Puerto Rico, USGS Misc. Invest. Ser., I-1153.

Brocard, G., C. Teyssier, W. J. Dunlap, C. Authemayou, T. Simon-Labric, N. Cacao-Chiquín, A. Guttiérrez-Orrego, and S. Morán-Ical (2011), Reorganization of a deeply incised drainage: Role of deformation, sedimentation, and groundwater flow, *Basin Res.*, *23*(6), 631–651.

Brocard, G., et al. (2012), Rates and processes of river network rearrangement during incipient faulting: The case of the Cahabón River, Guatemala, *Am. J. Sci.*, *312*, 449–507, doi:10.2475/05.2012.01.

Brocard, G., J. K. Willenbring, F. N. Scatena, and A. H. Johnson (2015), Effects of a tectonically-triggered wave of incision on Riverine Exports and Soil Mineralogy in the Luquillo Mountains of Puerto Rico, in Hydrochemistry of Tropical SMRs, edited by S. Goldsmith and Moyer R, *J. Appl. Geochem.*, *63*, 586–598.

Brown, E. T., R. F. Stallard, M. C. Larsen, G. M. Raisbeck, and F. Yiou (1995), Denudation rates determined from the accumulation of in situ-produced ^{10}Be in the Luquillo Experimental Forest, Puerto Rico, *Earth Planet. Sci. Lett.*, *129*(1), 193–202.

Brown, E. T., R. F. Stallard, M. C. Larsen, D. L. Bourlès, G. M. Raisbeck, and F. Yiou (1998), Determination of predevelopment denudation rates of an agricultural watershed (Cayaguas River, Puerto Rico) using in-situ-produced ^{10}Be in river-borne quartz, *Earth Planet. Sci. Lett.*, *160*, 723–728.

Buss, H. L., S. L. Brantley, F. N. Scatena, E. A. Bazilievskaya, A. Blum, M. Schulz, R. Jiménez, A. F. White, G. Rother, and D. Cole (2013), Probing the deep critical zone beneath the Luquillo Experimental Forest, Puerto Rico, *Earth Surf. Processes Landforms*, *38*, 1170–1186.

Carson, M. A., and M. J. Kirby (1972), *Hillslope Form and Process*, Cambridge Univ. Press, Cambridge, U. K.

Chabaux, F., E. Blaes, P. Stille, R. di Chiara Roupert, E. Pelt, A. Dosseto, L. Ma, H. L. Buss, and S. L. Brantley (2013), Regolith formation rate from U-series nuclides: Implications from the study of a spheroidal weathering profile in the Rio Icacos watershed (Puerto Rico), *Geochim. Cosmochim. Acta.*, *100*, 73–95.

Cook, K. L., J. M. Turowski, and N. Hovius (2013), A demonstration of the importance of bedload transport for fluvial bedrock erosion and knickpoint propagation, *Earth Surf. Processes Landforms*, *38*, 683–695.

Crosby, B., and K. X. Whipple (2006), Knickpoint initiation and distribution within fluvial networks: 236 waterfalls in the Waipaoa River, North Island, New Zealand, *Geomorphology*, *82*(1–2), 16–38, doi:10.1016/j.geomorph.2005.08.023.

de Lange, W. P., and V. G. Moon (2005), Estimating long-term cliff recession rates from shore platform widths, *Eng. Geol.*, *80*, 292–301.

Delvaux, D., and S. Sperner (2003), New aspects of tectonic stress inversion with reference to the TENSOR program, *Geol. Soc. London Spec. Publ.*, *212*, 75–100.

Dornbusch, U., D. A. Robinson, C. A. Moses, and R. B. Williams (2008), Temporal and spatial variations of chalk cliff retreat in East Sussex, 1873 to 2001, *Mar. Geol.*, *249*(3), 271–282.

Foley, M. G. (1980), Bedrock incision by streams, *Geol. Soc. Am. Bull.*, *91*, 2189–2213.

Frankel, K. L., F. J. Pazzaglia, and J. D. Vaughn (2007), Knickpoint evolution in a vertically bedded substrate, upstream-dipping terraces, and Atlantic slope bedrock channels, *Geol. Soc. Am. Bull.*, *119*, 476–486.

Garcia-Castellanos, D. (2007), The role of climate during high plateau formation. Insights from numerical experiments, *Earth Planet. Sci.. Lett.*, *257*, 372–390.

Giusti, E. V. (1978), Hydrogeology of the karst of Puerto, U.S. Geol. Surv. Prof. Pap., 1012.

Granger, D. E., and P. F. Muzikar (2001), Dating sediment burial with in situ-produced cosmogenic nuclides: Theory, techniques, and limitations, Earth Planet. *Sci. Lett.*, *188*, 269–281.

Gunnell, Y., M. Calvet, S. Brichau, A. Carter, J. P. Aguilar, and H. Zeyen (2009), Low long-term erosion rates in high-energy mountain belts: Insights from thermo-and biochronology in the Eastern Pyrenees, *Earth Planet. Sci. Lett.*, *278*(3), 208–218.

Harden, C. P., and P. D. Cruggs (2003), Infiltration on mountain slopes: A comparison of three environments, *Geomorphology*, *55*, 5–24.

Hayward, B. W., T. Cedhagen, M. Kaminski, and O. Gross (2015), World foraminifera database. [Available at http://www.marinespecies.org/foraminifera.]

Hayakawa, Y., and Y. Matsukura (2003), Recession rates of waterfalls in Boso Peninsula, Japan, and predictive equation, *Earth Surf. Processes Landforms*, *28*, 675–684.

House, M. A., B. P. Wernicke, and K. A. Farley (2001), Paleo-geomorphology of the Sierra Nevada, California, from U-Th/He ages in apatite, *Am. J. Sci.*, *301*, 77–102.

Hippolyte, J. C., P. Mann, and N. R. Grindlay (2005), Geologic evidence for the prolongation of active normal faults of the Mona rift into northwestern Puerto Rico, *Geol. Soc. Am. Spec. Publ.*, *385*, 161–171.

Humphrey, N. F., and P. L. Heller (1995), Natural oscillations in coupled geomorphic systems: An alternative origin for cyclic sedimentation, *Geology*, *23*(6), 499–502.

Jansen, J. D., D. Gabel, P. Bishop, S. Xu, C. Schnabel, and A. T. Codilean (2011), Does decreasing paraglacial sediment supply slow knickpoint retreat?, *Geology*, *39*(6), 543–546.

Jolly, W. T., E. G. Lidiak, J. H. Schellekens, and H. Santos (1998), Volcanism, tectonics, and stratigraphic correlations in Puerto Rico, in Tectonics and Geochemistry of the Northeastern Caribbean, *Geol. Soc. Am. Spec. Publ.*, *322*, pp. 1–34.

Kellerhals, R., and D. I. Bray (1971), Sampling procedures for coarse fluvial sediments, *J. Hydraul. Div.*, *97*, 1165–1180.

Kohl, C. P., and K. Nishiizumi (1992), Chemical isolation of quartz for measurement of in situ-produced cosmogenic nuclides, *Geochem. Cosmochim. Acta*, *56*, 3583–3587.

Laity, J. E., and M. C. Malin (1985), Sapping processes and the development of theatre-headed valley networks on the Colorado Plateau, *Geol. Soc. Am. Bull.*, *96*, 203–217.

Lal, D. (1991), Cosmic ray labeling of erosion surfaces: In situ nuclide production rates and erosion models, *Earth Planet. Sci. Lett.*, *104*, 424–439, doi:10.1016/0012-821X(91)90220-C.

Lamb, M. P., W. E. Dietrich, and L. S. Sklar (2008), A model for fluvial bedrock incision by impacting suspended and bed load sediment, *J. Geophys. Res.*, *113*, F03025, doi:10.1029/2007JF000915.

Larsen, M. C., A. J. Torrez-Sanchez, and I. M. Concepcion (1999), Slopewash, surface runoff and fine-litter transport in forest and landslide cars in humid-tropical steeplands, Luquillo experimental forest, Puerto Rico, *Earth Surf. Processes Landforms*, *24*, 481–502.

Larsen, M. C., Z. Liu, and X. Zou (2012), Effects of earthworms on slope wash, surface runoff, and fine-litter transport on a humid tropical forested hillslope, Luquillo experimental forest, Puerto Rico, in *Water Quality and Landscape Processes of Four Watersheds in Eastern Puerto Rico*, *Geol. Surv. Prof. Pap.*, 1789, 179–197.

Lavé, J., and J.-P. Avouac (2001), Fluvial incision and tectonic uplift across the Himalayas of central Nepal, *J. Geophys. Res.*, *106*(B11), 255,261–25,593.

Letortu, P., S. Costa, A. Bensaid, J. M. Cador, and H. Quénol (2014), Vitesses et modalités de recul des falaises crayeuses de Haute-Normandie (France): Méthodologie et variabilité du recul, *Géomorphologie*, *2*, 133–144.

Lobeck, A. K. (1922), The physiography of Porto Rico, *Sci. Surv. Porto Rico Virgin Islands*, *1*, 301–379.

Mackey, B. H., J. S. Scheingross, M. P. Lamb, and K. A. Farley (2014), Knickpoint formation, rapid propagation, and landscape response following coastal cliff retreat at the last interglacial sea-level highstand: Kaua'i, Hawai'i, *Geol. Soc. Am. Bull.*, *126*(7–8), 925–942.

Maidment, D. R. (2002), *Arc Hydro: GIS for Water Resources*, ESRI Press, Redlands, Calif.

Mann, J. F., F. Taylor, R. L. Edwards, and T. Ku (1995), Actively evolving microplate formation by oblique collision and sideways motion along strike-slip faults: An example from the northeastern margin of the Caribbean Plate, *Tectonophysics*, *246*, 1–69.

Meyerhoff, H. A. (1927), Tertiary physiographic development of Porto Rico and the Virgin Islands, *Bull. Geol. Soc. Am.*, *38*, 557–576.

Miller, J. R. (1991), The influence of bedrock geology on knickpoint development and channel-bed degradation along downcutting streams in south-central Indiana, *J. Geol.*, *99*, 591–605.

Miller, K. L., T. Szabó, D. J. Jerolmack, and G. Domokos (2014), Quantifying the significance of abrasion and selective transport for downstream fluvial grain size evolution, *J. Geophy. Res. Earth Surf.*, *119*, 2412–2429, doi:10.1002/2014JF003156.

Miller, T. E. (2004), Surface and subterranean drainage piracy, reorganization, and knickpoints of the Río Tanamá and Río Camuy, Puerto Rico: Presented at Geol. Soc. Am. Annual Meeting, Abstracts with Programs 36(5), 11.

Miller, T. E. (2007), Geologic controls, speleogenesis, and trends of Cueva Cucaracha (Rio Chico), Aguadilla, Puerto Rico, presented at 5th Congress of the Federación Espeleologica de America Latina y el Caribe, 91.

Mitchell, N. C., W. B. Dade, and D. G. Masson (2003), Erosion of the submarine flanks of the Canary Islands, *J. Geophys. Res.*, *108*(F1), 6002, doi:10.1029/2002JF000003.

Monroe, W. H. (1976), The karst landforms of Puerto Rico, *U.S. Geol. Surv. Prof. Pap.*, 899.

Monroe, W. H. (1980a), Geology of the middle Tertiary formations of Puerto Rico, *U.S. Geol. Surv. Prof. Pap.*, 953.

Monroe, W. H. (1980b), Some tropical landforms of Puerto Rico, *U.S. Geol. Surv. Prof. Pap.*, 1159.

Montgomery, D. R. (2004), Observations on the role of lithology in strath terrace formation and bedrock channel width, *Am. J. Sci.*, *304*(5), 454–476.

Moussa, M. T., G. A. Seiglie, A. A. Meyerhoff, and I. Taner (1987), The Quebradillas Limestone (Miocene-Pliocene) northern Puerto Rico, and tectonics of the northeastern Caribbean margin, *Geol. Soc. Am. Bull.*, *99*, 427–439.

Murphy, S. F., and R. F. Stallard (2012), Hydrology and climate of four watersheds in Eastern Puerto Rico, in Water Quality and Landscape Processes of Four Watersheds in Eastern Puerto Rico, *Geol. Surv. Prof. Pap.*, 1789, 43–84.

Nishiizumi, K., M. Imamura, M. W. Caffee, J. R. Southon, R. C. Finkel, and J. McAninch (2007), Absolute calibration of [10]Be AMS standards, *Nucl. Instrum. Meth. Phys. Res. Sect. B: Beam Interactions with Materials and Atoms*, *258*, 403–413.

Perron, J. T., and L. Royden (2012), An integral approach to bedrock river profile analysis, *Earth Surf. Processes Landforms*, *38*, 570–576.

Pike, A. W., F. N. Scatena, and E. E. Wohl (2010), Lithological and fluvial controls on the geomorphology of tropical montane stream channels in Puerto Rico, *Earth Surf. Processes Landforms*, *35*, 1402–1417, doi:10.1002/esp.1978.

Phillips, C. B., R. L. Martin, and D. J. Jerolmack (2013), Impulse framework for unsteady flows reveals superdiffusive bed load transport, *Geophys. Res. Lett.*, *40*, 1328–1333, doi:10.1002/grl.50323.

Porder, S., A. H. Johnson, X. Hao, G. Brocard, and S. Goldsmith (2015), Linking geomorphology, weathering and cation availability in the Luquillo Mountains of Puerto Rico, *Geoderma*, *249-250*, 100–110.

Renken, R. A., W. C. Ward, I. P. Gill, F. Gómez-Gómez, and J. Rodríguez-Martínez (2002), Geology and hydrogeology of the Caribbean islands aquifer system of the commonwealth of Puerto Rico and the US Virgin Islands, *U.S. Geol. Surv. Prof. Pap. 1419*, 1–139.

Richardson, K., and P. A. Carling (2005), A typology of sculpted forms in open bedrock channels, *Geol. Soc. Am. Spec. Pap.*, *392*, 1–108.

Riebe, C. S., J. W. Kirchner, and R. C. Finkel (2003), Long-term rates of chemical weathering and physical erosion from cosmogenic nuclides and geochemical mass balance, *Geochim. Cosmochim. Acta*, *67*(22), 4411–4427.

Rojas-Agramonte, Y., F. Neubauer, D. E. Garcia-Delgado, R. Handler, G. Friedl, and R. Delgado-Damas (2008), Tectonic evolution of the Sierra Maestra Mountains, S.E. Cuba, during Tertiary times: From arc-continent collision to transform motion, *J. South Am. Earth Sci.*, *26*, 125–151.

Schaller, M., F. von Blanckenburg, N. Hovius, and P. W. Kubik (2001), Large-scale erosion rates from in situ-produced cosmogenic nuclides in European river sediments, *Earth Planet. Sci. Lett.*, *188*, 441–458.

Schellekens, J., F. N. Scatena, L. A. Bruijnzeel, A. I. J. M. van Dijk, M. M. A. Groen, and R. J. P. van Hogezand (2004), Stormflow generation in a small rainforest catchment in the Luquillo Experimental Forest, Puerto Rico, *Hydrol. Proc.*, *18*(3), 505–530.

Seiders, V. M. (1971), Geologic map of the El Yunque quadrangle, Puerto Rico, U. S. Geol. Surv. Misc. Geol. Invest., Map I-658.

Seiglie, G. A., and M. T. Moussa (1975), Paleoenvironments of the Quebradillas Limestone (Tertiary), Northern Puerto Rico, and their geologic significance, *Am. Assoc. Petrol. Geol. Bull.*, *59*(12), 2314–2321.

Semmes, D. R. (1919), Geology of the San Juan district, scientific survey of Porto Rico and the Virgin Islands, New York Academy Sci., pp. 50–51.

Sklar, L., and W. E. Dietrich (1998), River longitudinal profiles and bedrock incision models: Stream power and the influence of sediment supply, in *Rivers of Rock: Fluvial Processes in Bedrock Channels, Geophys. Monogr. Ser.*, vol. 107, edited by K. J. Tinkler and E. E. Wohl, pp. 237–260, AGU, Washington, D. C.

Sklar, L. S., and W. E. Dietrich (2001), Sediment and rock strength controls on river incision into bedrock, *Geology*, *29*(12), 1087–1090.

Sklar, L. S., and W. E. Dietrich (2006), The role of sediment in controlling steady-state bedrock channel slope: Implications of the saltation–abrasion incision model, *Geomorphology*, *82*(1), 58–83.

Schumm, S. A. (1973), Geomorphic thresholds and complex response of drainage systems, in Fluvial Geomorphology, New York State Univ. Pub. Geomorph. Binghamton, edited by M. Morisawa, 299–310.

Simon, A., M. C. Larsen, and C. R. Hupp (1990), The role of soil processes in determining mechanisms of slope failure and hillslope development in a humid-tropical forest, eastern Puerto Rico, *Geomorphology*, *3*, 263–286.

Smoot, N. C. (1995), Mass wasting and subaerial weathering in guyot formation: The Hawaiian and Canary Ridges as examples, *Geomorphology*, *14*(1), 29–41.

Stallard, R. F. (2012), Weathering, landscape equilibrium, and carbon in four watersheds in Eastern Puerto Rico, in Water Quality and Landscape Processes of Four Watersheds in Eastern Puerto Rico, *Geol. Surv. Prof. Pap.*, 1789, 208–232.

Stanek, K. P., W. V. Maresh, and J. L. Pindell (2009), The geotectonic story of the northwestern branch of the Caribbean arc: Implications from structural and geochronological data of Cuba, in *The Origin and Evolution of the Caribbean Plate*, edited by K. H. James, M. A. Lorente, and J. L. Pindell, *Geol. Soc. London Spec. Publ.*, *328*, 361–398.

ten Brink, U. S. (2005), Vertical motions of the Puerto Rico Trench and Puerto Rico and their cause, *J. Geophys. Res.*, *110*, B06404, doi:10.1029/2004JB003459.

ten Brink, U. S., S. Marshak, and J.-L. Granja-Bruña (2009), Bivergent thrust wedges surrounding oceanic island arcs: Insight from observations and sandbox models of the northeastern Caribbean plate, *Geol. Soc. Am. Bull.*, *121*, 1522–1536, doi:10.1130/B26512.1.

Troester, J. W. (1994), The geochemistry, hydrogeology and geomorphology of the Río Camuy drainage basin, Puerto Rico, PhD thesis, Pennsylvania State Univ., State College, Pa.

Tucker, G. E., and K. X. Whipple (2002), Topographic outcomes predicted by stream erosion models: Sensitivity analysis and inter-model comparison, *J. Geophys. Res.*, *107*(B9), 2179, doi:10.1029/2001JB000162.

Turner, B. F., R. F. Stallard, and S. L. Brantley (2003), Investigation of in situ weathering of quartz diorite bedrock in the Río Icacos basin, Luquillo Experimental Forest, Puerto Rico, *Chem. Geol.*, *202*, 313–341.

Turowski, J. M., C. R. Wyss, and A. R. Beer (2015), Grain size effects on energy delivery to the streambed and links to bedrock erosion, *Geophys. Res. Lett.*, *42*, 1775–1780, doi:10.1002/2015GL063159.

van Gestel, J.-P., P. Mann, J. F. Dolan, and N. R. Grindlay (1998), Structure and tectonics of the upper Cenozoic Puerto Rico-Virgin Islands carbonate platform as determined from seismic reflection studies, *J. Geophys. Res.*, *103*(B12), 30,505–30,530, doi:10.1029/98JB02341.

van Gestel, J.-P., P. Mann, N. R. Grindlay, and J. F. Dolan (1999), Three-phase tectonic evolution of the northern margin of Puerto Rico as inferred from an integration of seismic reflection, well, and outcrop data, *Marine Geol.*, *161*, 257–286.

van der Beek, P., J. Van Melle, S. Guillot, A. Pêcher, P. W. Reiners, S. Nicolesci, and M. Latif (2009), Eocene Tibetan plateau remnants preserved in the northwest Himalaya, *Nat. Geosci.*, *2*, 364–368.

Wakabayashi, J., and T. L. Sawyer (2001), Stream incision, tectonics, uplift, and evolution of topography of the Sierra Nevada, California, *J. Geol.*, *109*, 539–562.

Warrick, J. A., D. M. Rubin, P. Ruggiero, J. N. Harney, A. E. Draut, and D. Buscombe (2009), Cobble Cam: Grain-size measurements of sand to boulder from digital photographs and autocorrelation analyses, *Earth Surf. Processes Landforms*, *34*, 1811–1821.

Weissel, J. K., and M. A. Seidl (1998), Inland propagation of erosional escarpments and river profile evolution across the southeast Australian passive continental margin, in *Rivers Over Rock: Fluvial Processes in Bedrock Channels, Geophys. Monogr. Ser.*, vol.107, edited by K. Tinkler and E. Wohl, pp. 189–206, AGU, doi:10.1029/GM107p0189.

Whipple, K. X., and B. J. Meade (2006), Orogen response to changes in climatic and tectonic forcing, *Earth Planet. Sci. Lett.*, *243*(1), 218–228.

Whipple, K. X., G. S. Hanckock, and R. S. Anderson (2000), River incision into bedrock: Mechanics and relative efficacy of plucking, abrasion and cavitation, *Geol. Soc. Am. Bull.*, *112*, 490–503.

White, A. F., A. E. Blum, M. S. Schulz, D. V. Vivit, D. A. Stonestrom, M. Larsen, S. F. Murphy, and D. Eberl (1998), Chemical weathering in a tropical watershed, Luquillo Mountains, Puerto Rico: I. Long-term versus short-term weathering fluxes, *Geochim. Cosmochim. Ac.*, *62*(2), 209–226.

Willett, S. D., and M. T. Brandon (2002), On steady states in mountain belts, *Geology*, *30*(2), 175–178.

Willenbring, J. K., N. M. Gasparini, B. T. Crosby, and G. Brocard (2013), What does a mean means? The temporal evolution of detrital cosmogenic denudation rates in transient landscapes, *Geology*, *41*, 1215–1218.

Wohl, E. E. (1998), Bedrock channel morphology in relation to erosional processes, in *Rivers Over Rock: Fluvial Processes in Bedrock Channels, Geophys. Monogr. Ser.*, vol. 107, edited by K. Tinkler, and E. Wohl, pp. 133–151, AGU, Washington, D. C.

Wolman, M. G. (1954), A method of sampling coarse river-bed material, *EOS Trans. AGU*, *35*(6), 951–956.

Yang, R., S. D. Willett, and L. Goren (2015), In situ low-relief landscape formation as a result of river network disruption, *Nature*, *520*(7548), 526–529.